



Cite this: *Chem. Soc. Rev.*, 2021, 50, 4141

## Advances in multiplexed techniques for the detection and quantification of microRNAs

Thomas Jet,<sup>ab</sup> Guillaume Gines,<sup>\*b</sup> Yannick Rondelez <sup>b</sup> and Valérie Taly <sup>\*a</sup>

MicroRNA detection is currently a crucial analytical chemistry challenge: almost 2000 papers were referenced in PubMed in 2018 and 2019 for the keywords "miRNA detection method". MicroRNAs are potential biomarkers for multiple diseases including cancers, neurodegenerative and cardiovascular diseases. Since miRNAs are stably released in bodily fluids, they are of prime interest for the development of non-invasive diagnosis methods, such as liquid biopsies. Their detection is however challenging, as high levels of sensitivity, specificity and robustness are required. The analysis also needs to be quantitative, since the aim is to detect miRNA concentration changes. Moreover, a high multiplexing capability is also of crucial importance, since the clinical potential of miRNAs probably lays in our ability to perform parallel mapping of multiple miRNA concentrations and recognize typical disease signature from this profile. A plethora of biochemical innovative detection methods have been reported recently and some of them provide new solutions to the problem of sensitive multiplex detection. In this review, we propose to analyze in particular the new developments in multiplexed approaches to miRNA detection. The main aspects of these methods (including sensitivity and specificity) will be analyzed, with a particular focus on the demonstrated multiplexing capability and potential of each of these methods.

Received 7th August 2020

DOI: 10.1039/d0cs00609b

rsc.li/chem-soc-rev

<sup>a</sup> Centre de Recherche des Cordeliers, INSERM, Sorbonne Université, Université de Paris, CNRS SNC5096, Equipe Labellisée Ligue Nationale Contre le Cancer, F-75006 Paris, France. E-mail: valerie.taly@parisdescartes.fr; Tel: +33 170 649 954

<sup>b</sup> Laboratoire Gulliver, UMR7083 CNRS, ESPCI Paris, Université Paris Sciences et Lettres, 10 Rue Vauquelin, 75005 Paris, France. E-mail: guillaume.gines@espci.fr



**Thomas Jet**

Thomas Jet obtained his chemical engineering degree from ESPCI Paris in 2016. He completed a MS in biochemistry at Paris Diderot University and Pasteur Institute in 2017. He is now a PhD student at Université de Paris and ESPCI Paris. His research focuses on microRNA detection using DNA-based chemical networks.



**Guillaume Gines**

Guillaume Gines received his PhD in chemical biology in 2013, working on the development of biosensors of DNA repair enzymes. Until 2016, he was a postdoctoral fellow in the Fujii laboratory (U. Tokyo), investigating the emergence of collective behaviors in large populations of DNA-programmed particles. He then moved to Paris to work on the development of microRNA detection technologies, spanning concepts from molecular

programming combined with microfluidics. Since 2020, he owns a CNRS research position at ESPCI Paris, PSL Research University. His research revolves around DNA nanotechnology and molecular programming, from their fundamental demonstrations to applications in diagnostics and biotechnology.



# 1 Interest and challenges of miRNA detection

MicroRNAs (miRNAs) are a class of short non-coding RNAs of about 19 to 25 nucleotides. They were first discovered in 1993 in *Caenorhabditis elegans*<sup>1</sup> and are said to be responsible for the post-transcriptional gene expression regulation of more than 60% of human protein-coding genes.<sup>2</sup> This regulatory process, called RNA interference (RNAi), was first described in 1998 by Andrew Fire and Craig Mello,<sup>3</sup> who were awarded the 2006 Nobel Prize in Medicine and Physiology.

In order to regulate gene expression, miRNAs form complexes with protein GW182 and one of the proteins of the Argonaute (AGO) family.<sup>4,5</sup> This complex is known as the miRNA-Induced Silencing Complex (miRISC). In this complex, the miRNA is used for target recognition through base pairing, whereas proteins actively induce repression.<sup>6</sup> Two main mechanisms of the miRISC complex are proposed (Fig. 1): in most cases, the miRNA binds the 3' untranslated region (UTR) thanks to a region known as the miRNA "seed", located between the second and the seventh nucleotides. The RISC proteins then recruit factors inhibiting mRNA translation and promoting mRNA deadenylation.<sup>4</sup> Another mechanism of action of miRISC involves the complete binding of the miRNA inside the coding region of the gene, which leads to mRNA cleavage by the AGO protein.<sup>7</sup> The shortness of the miRNA-recognition site on the 3' UTR of the mRNAs explains how only a few thousands miRNAs can regulate the expression of more than half of human genes.

The biogenesis of miRNAs is initiated in the nucleus, as miRNA genes are transcribed by RNA polymerase II into a primary miRNA (pri-miRNA) (Fig. 2). The pri-miRNA is generally over 1 kb long and partially hairpin-shaped, with single-stranded

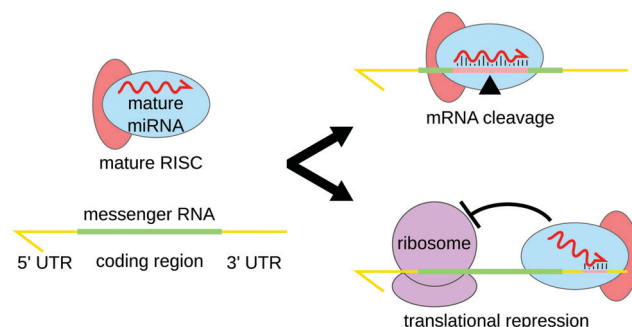


Fig. 1 The two main miRNA-induced pathways for post-transcriptional regulation. Complete binding of the miRNA to the coding region of the mRNA leads to the cleavage of the mRNA by the proteins of the RISC complex. Alternatively, the "seed" region of the miRNA, typically located between the second and seventh nucleotide hybridizes to one of the untranslated regions (most commonly 3' UTR). This partial binding triggers the recruitment of translation-inhibiting factors and/or destabilizes the mRNA by promoting its deadenylation.

3' and 5' ends. The mature miRNA sequence is part of the stem. Still inside the nucleus, this pri-miRNA undergoes maturation by the Microprocessor complex composed of nuclear RNase III Drosha and cofactor DGCR8.<sup>6</sup> Drosha cleaves the pri-miRNA and releases a 65 bases long hairpin-shaped RNA called precursor-miRNA (pre-miRNA). The pre-miRNA is exported in the cytoplasm, where it undergoes a second maturation step by Dicer endonuclease. Dicer cleaves pre-miRNA near both ends of the loop, releasing a duplex of small RNAs. This duplex is loaded onto an AGO protein to form a pre-RISC. The duplex is then unwinded by a helicase and only one of the RNAs remains in the complex, forming a mature RNA-induced silencing complex. For a more complete overview of miRNA biogenesis and physiological role, we refer the reader to other reviews.<sup>6,8,9</sup>



**Yannick Rondelez**

*Yannick Rondelez has a background in chemistry, single molecule biophysics, microfluidic and enzymology.*

*He develops new approaches to manipulate information in molecular systems, including those with non-linear dynamics, or implementing neural architectures. He is an expert in new chemical approaches based on synthetic DNA, high throughput methods using micro-compartmentalization and sequencing, and complex bio-processes. He currently works on the applications of artificial molecular circuits, including advanced diagnostics and artificial evolution.*



**Valérie Taly**

*Valérie Taly is a CNRS research director, group leader of the Translational Research And Microfluidics group and deputy director of the MEPPOT team (personalized medicine, pharmacogenomics and therapeutic optimization) in the Cordeliers Research Center. Her group performs interdisciplinary researches aiming at developing and validating microfluidic tools for cancer research in close collaboration with clinicians and researchers in oncology. Her research is dedicated to the development of original tools and procedures, with a specific focus on droplet-based microfluidics, for the non-invasive detection of cancer biomarkers and the highlighting of new Biomarkers with applications in personalized medicine, cancer recurrence detection and diagnostics.*



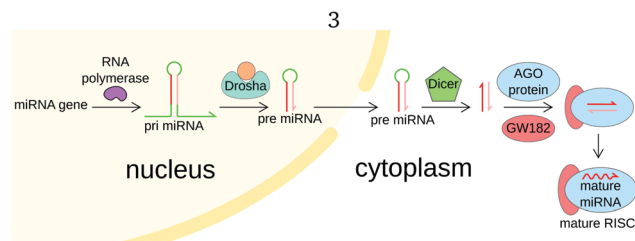


Fig. 2 Simplified miRNA biogenesis pathway. The miRNA gene is transcribed into a 1 kb-long primary miRNA (pri-miRNA). The pri-miRNA then undergoes two successive maturation, first forming an hairpin-shaped precursor miRNA (pre-miRNA) and then an RNA duplex composed of the miRNA and its complementary sequence. The complex binds a protein of the Argonaute (AGO) family and is unwound by a helicase, releasing the complementary strand. The mature miRNA remains bound to the complex composed of AGO and other proteins, such as GW182, called the miRNA-induced silencing complex (miRISC).

The role of miRNAs in cancer was first evidenced by Croce's group in 2002 when they discovered that a genomic region on which were located two miRNA genes was commonly deleted in chronic lymphocytic leukemia.<sup>10</sup> Since then, a plethora of disease-related miRNA dysregulations have been reported, not only in cancer,<sup>11</sup> but also for Parkinson's disease,<sup>12</sup> diabetes<sup>13</sup> and cardiovascular diseases,<sup>14</sup> among others. The causes of these dysregulations are for example gene deletions<sup>10,15</sup> or amplifications<sup>16,17</sup> and defects in miRNA transcriptional control<sup>18–20</sup> or biogenesis machinery.<sup>21,22</sup> In cancer, due to their gene expression-regulating role, miRNA dysregulations could contribute to most of the cancer hallmarks. Among countless examples, miR92a's upregulation has been described as promoting cell proliferation,<sup>23</sup> miR21 was found upregulated in lung cancer and inducing apoptosis resistance,<sup>24</sup> whereas miR203 downregulation was observed in metastatic breast cancer cells.<sup>11</sup>

Tumor tissue biopsy is currently the main biomarker analysis method for cancer diagnostics. This procedure however presents serious drawbacks, such as limited capacities to recapitulate tumor heterogeneity, high cost and invasiveness. Moreover it is also not appropriate for tumor real time characterization, which could be of great interest for patient follow up and treatment management. To circumvent these limitations, liquid biopsies are being developed. Liquid biopsy relies on the analysis of circulating biomarkers (including circulating tumor DNA, circulating tumor cells, proteins and miRNAs) in bodily fluids, such as blood or urine. MiRNAs have been shown to be released by healthy and tumor cells in the bloodstream and other biofluids.<sup>25</sup> These circulating miRNAs are thought to be not only passively released by apoptotic or necrotic cells, as it has mainly been described for ctDNA, but also actively secreted by living cells in extracellular vesicles. Studies suggest that secreted miRNAs could be addressed and delivered to specific cells. Once inside target cells, recovered miRNAs would modify the gene expression pattern, thus playing a long distance cell-to-cell signaling role.<sup>26</sup> Moreover, released miRNAs are protected, by conjugation to RNA-binding proteins such as AGO2 or high-density lipoprotein (HDL),<sup>5</sup> and are thus very stable even under

harsh conditions.<sup>27</sup> These characteristics make miRNAs very promising biomarkers for liquid biopsy strategies.

### 1.1 Challenges for miRNA detection

In spite of their attractiveness as biomarkers, several challenges need to be addressed in order to apply miRNA detection to cancer diagnosis. First, miRNAs are very short sequences, displaying a high level of homology, especially if they belong to the same family: the Let-7 miRNA family, involved in numerous pathologies including cancers, is comprised of 10 miRNAs sharing the same seed and most other nucleotides.<sup>28</sup> Let-7a and Let-7e, for example, are perfectly identical with the exception of their 9th nucleotide. Hence, a very high level of specificity is required to selectively quantify each miRNA.

MiRNAs only represent 0.01% of total RNA mass,<sup>29</sup> and additionally need to be detected from highly complex media. In blood plasma, the concentrations of miRNAs are in the sub-picomolar (pM) range.<sup>27,30</sup> In addition to sufficient sensitivity, miRNA detection methods need to display a dynamic range spanning at least four orders of magnitude.

The aim of a miRNA-based liquid biopsy is to detect miRNA concentrations changes, as both healthy and tumor cells release miRNAs, but in different relative quantities. Since these dysregulations may be subtle, the accuracy and precision of the assay is thus of utmost importance.

### 1.2 Importance of multiplexed detection

The study of the dysregulation of single miRNAs is, in most cases, insufficient for a reliable diagnosis. Some members of the Let-7 family, which work as inhibitors of cell growth, are down-regulated in different cancers, such as lung, breast and cervical cancers.<sup>31</sup> Similarly, miR-21, an apoptosis inhibitor, is found upregulated in glioblastoma, B-cell lymphoma and ovarian cancer, among others.<sup>32</sup> Consequently, the diagnostic, predictive and prognostic potential of miRNAs is most likely the determination of miRNA-signatures associated to a disease with which a patient miRNA profile can be compared.<sup>33</sup> A plethora of such signatures were described for both diagnostic<sup>34–36</sup> and prognostic applications.<sup>37–39</sup> The determination of disease signatures opens the way for diagnosis, which requires the quantification of multiple miRNAs in order to establish the miRNA profile of the patient. Such profiles can be determined either by running multiple single-plex detection reactions or a single multiplex reaction. In the case of parallel single-plex reactions, the sample is splitted in aliquots, one for each miRNA target. The required amount of sample thus increases proportionally to the number of miRNA targets, which is not the case of multiplexed detection methods. Alternatively, the sample can be diluted. Both of these strategies come at the cost of lowered sensitivity. Additionally, performing multiple single-plex assays in parallel significantly increases the workload, the cost and error risks. For all these reasons, the development of multiplex techniques has drawn considerable research efforts (Fig. 3).



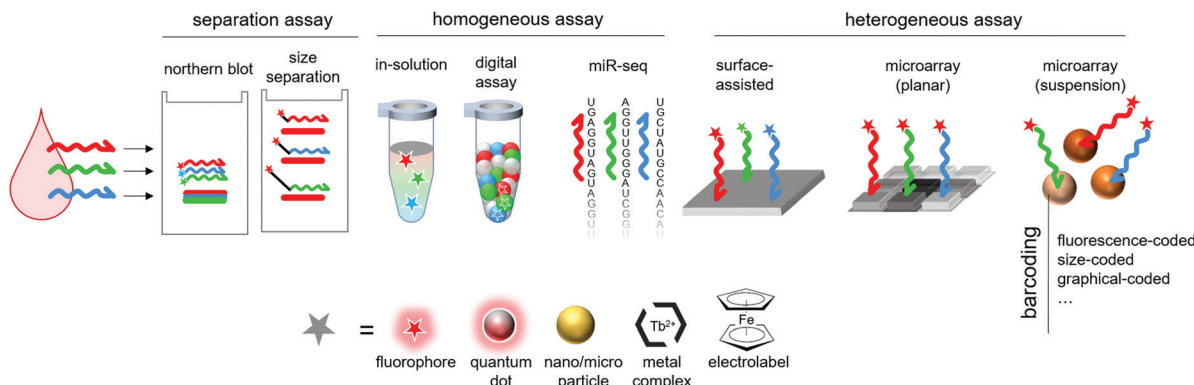


Fig. 3 Schematic representation of the approaches to multiplex miRNA detection presented in this review.

## 2 Amplification techniques applied to miRNA detection

The detection of miRNA targets, present in concentrations within the 1–100 femtomolars (fM) range, requires a high sensitivity and accuracy. The amplification of the target sequence or of an intermediate molecule is in most cases mandatory to detect such diluted targets by conventional read-out strategies, such as fluorescence. While the pool of DNA amplification chemistries comprises a plethora of techniques, most of them are not fitted for the amplification of short RNA sequences such as miRNAs.

Here we briefly describe conventional amplification methods and the developments that were made in an attempt to adapt these methods to the amplification of miRNAs and to increase the accuracy and the specificity of the quantification. For a more detailed overview of nucleic acids amplification techniques applied to miRNA detection, we refer the readers to another review.<sup>40</sup>

### 2.1 RT-qPCR

Of all miRNA detection techniques herein presented, RT-qPCR is undoubtedly considered as the gold-standard method. It allows for the detection of miRNA targets down to the attomolar (aM) range<sup>41,42</sup> and displays single-nucleotide specificity<sup>43</sup> while being relatively low-cost. RT-qPCR also features a wide dynamic range, spanning up to 8 orders of magnitude.

Quantification of RNA molecules by RT-qPCR, in general, comprises two steps: (i) Reverse Transcriptase (RT) is first used to synthesize the complementary DNA (cDNA) of the RNA target. (ii) this cDNA is then amplified by PCR thanks to a thermostable DNA polymerase and a pair of primers. The amplification is monitored in real-time by fluorescence, using either a double-stranded DNA specific dye (e.g. SYBR Green I) or specific fluorescence probes (e.g. hydrolysis or molecular beacon probes) labeled with orthogonal dyes in the case of multiplex RT-qPCR (*cf.* Section 3.2.1) (Fig. 4b). The target is quantified by measuring the number of temperature cycles necessary to cross a fluorescence threshold ( $C_q$ ) and comparing it to a standard range of samples of known concentrations.

Adapting qPCR to miRNA quantification requires some ingenuity. Indeed, RT-qPCR was initially developed to quantify

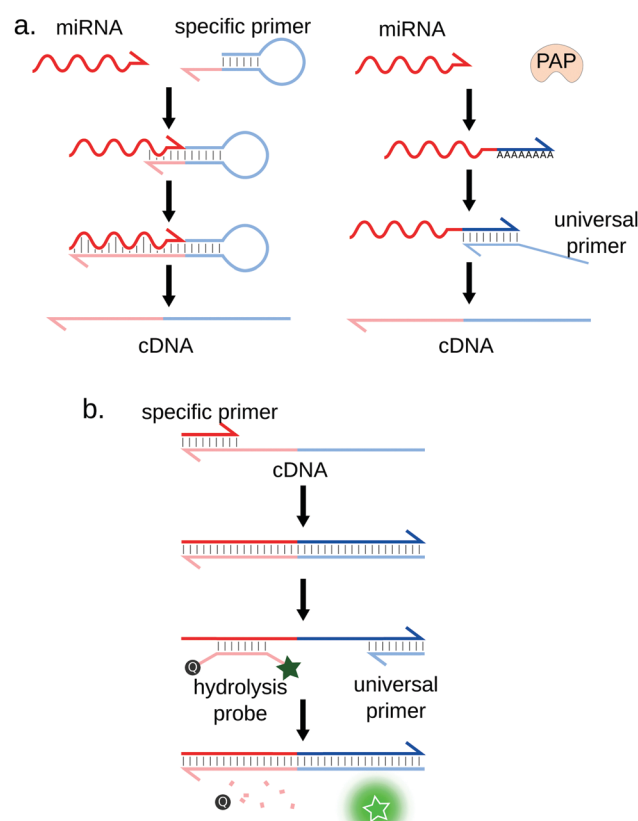


Fig. 4 Principle of RT-qPCR. (a) Reverse-transcription strategies. Left: The miRNA is reverse-transcribed using a miRNA-specific hairpin-shaped primer that partially hybridizes to the miRNA 3' end. Right: The 3' ends of all miRNAs are extended using the poly(A) polymerase (PAP). This allows the reverse transcription of all miRNAs using a universal primer. (b) The produced complementary DNA (cDNA) strands are quantified by qPCR, using a miRNA-specific and an universal primer.

long RNA sequences: typical PCR primers are approximately 20 bases long, which is the size of a full miRNA. This problem was solved by designing stem-loop<sup>41</sup> or linear<sup>44</sup> RT primers partially complementary to the miRNA (Fig. 4a, left) or by using the poly(A) polymerase (PAP)<sup>42</sup> (Fig. 4a, right). Although convenient, this method may reduce the specificity and sensitivity of



the assay.<sup>40</sup> This observation is however contradicted by a study by Mestdagh *et al.*,<sup>45</sup> where the authors systematically analysed seven RT-qPCR kits. They showed that minimal cross-reactivity is obtained using the polyA strategy, in combination with LNA-modified universal RT primer. Another limitation of miRNA RT-qPCR is that the interval of melting temperatures ( $T_m$ ) of the miRNA-specific primer/miRNA duplex is rather large due to the heterogeneous GC content of miRNAs. According to Benes *et al.*, the sensitivity is reduced if the  $T_m$  is below 55 °C, which can be the case for GC-poor miRNA sequences.<sup>46</sup> Moreover, the RT step efficiency can also depend on the miRNA sequence or structure, which has been shown to introduce biases in the transcribed cDNA library.<sup>47,48</sup>

RT-related biases can be reduced by using two-tailed primers,<sup>49</sup> or by replacing the RT by a miRNA-induced ligation step.<sup>50,51</sup> The ligated oligonucleotide is the cDNA strand that will be then quantified by qPCR. This ligation step is however also most likely prone to sequence-specific biases, as shown in the context of library preparation for small RNA sequencing.<sup>52</sup> Two-tailed primers and ligation-mediated qPCR also increase the specificity of the detection.<sup>49,53</sup> In the case of ligation-mediated qPCR, the choice of the ligase is especially important to specificity. Jin and coworkers demonstrated a detection of several members of the Let-7 family with excellent specificity by using the SplintR ligase instead of the commonly used T4 ligase.<sup>53</sup> This strategy has also been adapted to recombinase polymerase amplification (RPA).<sup>54</sup>

As it was already mentioned, qPCR-based measurement only provides a relative quantification of the sample, with respect to a calibration curve established from standard samples. This approach may thus introduce quantification biases (e.g. due to the presence of PCR inhibitors in the sample).

## 2.2 Rolling circle amplification

Rolling circle amplification (RCA) was originally designed by Kool's group as a method for the linear amplification of single-stranded RNA<sup>55</sup> or DNA.<sup>56</sup> The amplification uses circular single-stranded DNA as a template. Once a forward primer (P1, the miRNA in this case) hybridizes to the circular template, it is elongated by a DNA polymerase. The polymerase progresses around the circular template multiple times, producing a long concatemer composed of numerous copies of the sequence complementary to the template (Fig. 5).

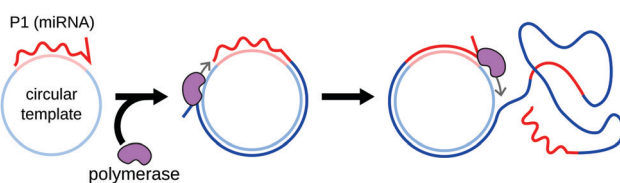


Fig. 5 Principle of RCA. The miRNA hybridizes to a circular DNA template, and acts as a primer for elongation by a DNA polymerase. The polymerase keeps progressing around the circular template, producing a long DNA strand composed of repeats of the same sequence. Amplification is reported by the hybridization of fluorescent probes complementary to the repeat sequence.

RCA was first applied to miRNA detection by Jonstrup *et al.*<sup>57</sup> The sensitivity of the method was low, due to its northern blot readout. Interestingly, the assay relied on linear detection probes that were circularized by ligation upon miRNA hybridization, therefore increasing specificity. The use of SplintR ligase,<sup>58,59</sup> dumbbell probes<sup>60</sup> or graphene-oxide nanosheets<sup>61</sup> further improved detection specificity. The sensitivity of RCA-based detection can be enhanced by adding additional primers, turning the concatemer into a template for further amplification.<sup>62</sup> RCA can also be converted to an exponential amplification method by integrating nicking enzyme recognition sites to the template sequence, as demonstrated for miRNA detection by Liu *et al.*<sup>63</sup>

## 2.3 Exponential amplification reaction

Exponential amplification reaction (EXPAR) was designed by Galas and coworkers as an alternative to PCR.<sup>64,65</sup> EXPAR allows the amplification of a nucleic acid sequence using a DNA template, a DNA polymerase and a nicking enzyme<sup>66</sup> (Fig. 6). The DNA template is composed of two miRNA-complementary sequences separated by a nicking enzyme recognition site. Upon hybridization, the miRNA is used as a primer for elongation. The nicking enzyme then recognizes its specific site, and cleaves only the miRNA-containing strand, releasing a DNA analog of the miRNA. This DNA strand in turn hybridizes to another template, which generates more miRNA analogs. The miRNA sequence is therefore exponentially amplified.

While being an efficient signal-amplification method (10<sup>6</sup> to 10<sup>9</sup>-fold amplification),<sup>67</sup> EXPAR is however prone to unspecific amplification, which limits its sensitivity.<sup>68,69</sup> This problem has been addressed by Montagne and coworkers, who introduced an additional template (referred as pseudotemplate) that drives the deactivation of unspecifically produced triggers,<sup>70</sup> allowing accurate miRNA quantification using a digital readout

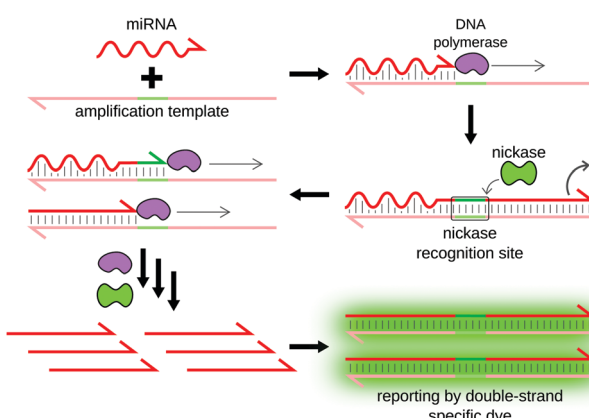


Fig. 6 Principle of EXPAR. The miRNA is captured by a DNA template composed of two miRNA-complementary sequences separated by a nicking enzyme recognition site. Binding of the miRNA initiates the production of multiple DNA analogs of the miRNA following polymerization/nicking cycles. The produced miRNA analogs are released in the solution and can in turn initiate the production of more analogs, resulting in exponential amplification.



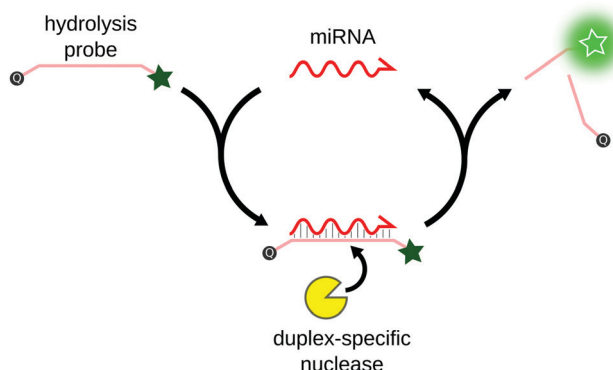


Fig. 7 Principle of DSNSA. Hybridization of the miRNA to a complementary DNA hydrolysis probe forms a RNA/DNA duplex. The duplex-specific nuclease recognizes the duplex and selectively degrades the probe, producing fluorescence. The miRNA remains untouched and is free to bind to another hydrolysis probe, triggering its degradation.

(see Section 3.2.3).<sup>71</sup> Additionally, the specificity of the assay by Jia's group within the Let7 family was rather low: the chemical network designed for Let7-a detection was triggered almost simultaneously by Let7-a and Let7-e. Several groups adapted the original EXPAR design in order to improve the specificity, such as using dumbbell or hairpin-shaped probes.<sup>72,73</sup>

#### 2.4 Duplex-specific nuclease signal amplification

Duplex-specific nuclease signal amplification (DSNSA) is commonly used for multiplex miRNA detection. Originally isolated from the Kamchatka crab,<sup>74</sup> the duplex-specific nuclease (DSN) was first characterized as an exonuclease that specifically degrades double-stranded DNA. Anisimova *et al.* later demonstrated that in the presence of DNA:RNA duplexes, DSN specifically degrades the DNA strand, leaving the RNA strand untouched.<sup>75</sup> Based on this property, Yin *et al.* first applied DSN for the simultaneous detection of 3 miRNAs with sub-pM sensitivity.<sup>76</sup> The assay was based on the hybridization of hydrolysis DNA probes on the miRNA, thus forming a DNA:RNA duplex. The hydrolysis probe was preferentially degraded by DSN, and the unaffected miRNA was free to hybridize to another probe, resulting in linear signal amplification (Fig. 7). The sensitivity of the assay was improved using different reporter probes, such as molecular beacons<sup>77</sup> or G-quadruplex specific probes.<sup>78</sup> Alternatively to DSN, CRISPR-associated nucleases (Cas)<sup>79</sup> or T7 exonuclease<sup>80</sup> were successfully applied to similar methods for miRNA detection.

#### 2.5 Enzyme-free amplification techniques

Contrary to most other amplification methods presented herein, hybridization chain reaction (HCR) and catalyzed hairpin amplification (CHA) are enzyme-free amplification techniques. First described by Dirks and Pierce,<sup>81,82</sup> HCR only uses two short DNA hairpins (H1 and H2) and a single-stranded initiator hairpin (Fig. 8). The loop region of the initiator hybridizes to the target. The 5' and 3' ends of the initiator become available and hybridize to H1, opening it in the process. The part of H1 that remains single-stranded is

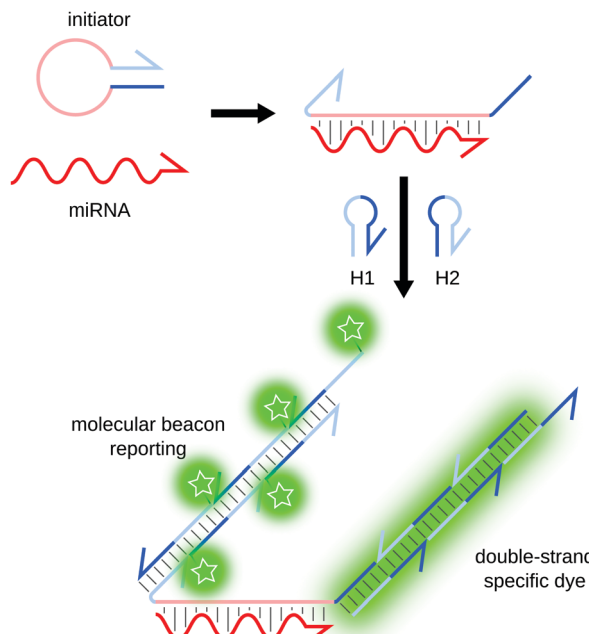


Fig. 8 Principle of HCR. The hybridization of the miRNA to the initiator strand triggers sequential concatenation of hairpins H1 and H2, forming long regions of double-stranded DNA. The amplification can be monitored by a double-strand specific dye or by using molecular beacons as H1 and H2.

complementary to H2, which in turn opens and binds H1, resulting in the sequential concatenation of H1 and H2. The amplification can be monitored by fluorescence using molecular beacons as H1 and H2<sup>83</sup> or thanks to an intercalating dye.<sup>84</sup> This technique was applied by Pierce's team for the detection of mRNAs<sup>83,85</sup> and miRNAs,<sup>86</sup> with a limit of detection (LOD) of 25 attomoles (amol).

Developed by the same team, CHA also relies on toehold-mediated strand displacement.<sup>87</sup> The nucleic acid target triggers the opening of a first hairpin by hybridizing in the stem region. The target is then displaced by the binding of a second hairpin, and is thus recycled in the process. CHA can be coupled to various readout strategies, and provides an amplification ratio of around 100-fold.<sup>87-90</sup>

### 3 Multiplexed miRNA detection

#### 3.1 Separation techniques

**3.1.1 Northern blot and size-separation gel-based techniques.** Northern blotting (NB) is a well-established miRNA detection method, for example involved in the first identification of a miRNA.<sup>1</sup> In this method, cells RNA extracts first undergo a size-separation step on a denaturing polyacrylamide gel (Fig. 9). Separated RNAs are then fixed on a membrane, on which sequences of interest are labeled by hybridization of complementary DNA probes. Historically radiolabeled with <sup>32</sup>P, these probes are now more commonly labeled using fluorescent or chemiluminescent dyes.



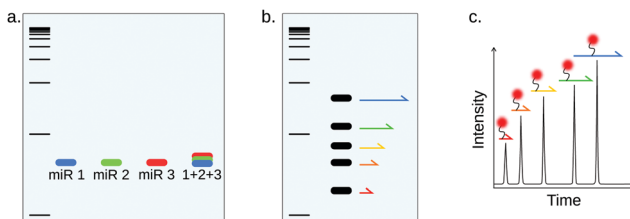


**Fig. 9** Multiplex miRNA detection strategies based on separation techniques. Since the size distribution of miRNAs is very narrow, miRNAs can not be directly separated based on size. Multiplex detection is however possible by using miRNA-specific detection probes (a), or by using the miRNA to generate size-coded DNA molecules that can be separated on slab gels (b) or by capillary electrophoresis (c).

Although it has been described as robust and reliable, NB is a cumbersome and time-consuming technique. Since gel electrophoresis cannot distinguish different sequences of the same molecular weight, as is the case for miRNAs, specificity relies only on probe hybridization, resulting in rather poor specificity and sensitivity. Both sensitivity and specificity can be improved by using locked nucleic acid (LNA)-modified probes.<sup>91</sup> Additionally, target quantitation is only relative and lacks accuracy.<sup>92</sup>

NB can be implemented into a multiplex miRNA detection method using color-coded detection probes (Fig. 9a), as was demonstrated by Schwarzkopf *et al.*<sup>86</sup> Interestingly, NB was in this work coupled to HCR amplification in order to improve sensitivity (100 amol). This multiplexing strategy is however limited by the availability of spectrally-resolved fluorescent probes.

In spite of the narrow size distribution of miRNAs, size-separation can be useful for multiplex miRNA detection by using the miRNAs to generate size-coded molecules (Fig. 9b). For example, Arefian *et al.* used miRNAs as a scaffold for the ligation of 2 miRNA-specific DNA sequences, one of which is of different length depending on the target miRNA.<sup>93</sup> The method allowed the simultaneous detection of 9 miRNAs of the Let-7 family, also showing great specificity, but rather low sensitivity (1 pM). Chandrasekaran and coworkers proposed another method, based on agarose gel separation.<sup>94</sup> This assay allows miRNA detection using only a double-stranded DNA probe with two miRNA-specific overhangs. The presence of the miRNA brings the 2 overhangs together, forcing the double-stranded DNA probe to form a loop. In this method, the barcoding strategy is only based on the distance between the two overhangs, which defines the size of the loop once the miRNA is captured and allows electrophoresis separation. The authors demonstrated multiplexing for up to five targets as well as single-nucleotide specificity, with a LOD around 100 fM.

**3.1.2 Capillary electrophoresis.** Also a size-based separation technique, capillary gel electrophoresis monitors the time needed for a molecule migrating in a gel-filled capillary to reach a detector (Fig. 9c). As for aforementioned slab gel techniques, multiple miRNAs can be indirectly detected by generating miRNA-specific size coded molecules. Jiang *et al.* demonstrated an amplification-free method based on the hybridization of target miRNAs to a capture probes presenting a poly(A) tail of different lengths, allowing separation based on the molecular

weight of the duplex.<sup>95</sup> An amplification step, such as PCR,<sup>96</sup> DSNSA<sup>97</sup> or EXPAR<sup>98</sup> can be added prior to separation to improve sensitivity. In terms of multiplexing, Na *et al.* managed to detect up to 8 miRNAs simultaneously using conformation-sensitive separation (single strand conformation polymorphism, CE-SSCP),<sup>98</sup> demonstrating the multiplexing potential of these methods. High-performance liquid chromatography (HPLC) was also used in a similar assay coupled to DSNSA, displaying sub-fM sensitivity.<sup>99</sup>

### 3.2 Homogeneous multiplex detection

Most conventional miRNA detection methods are fully realized in solution, such as RT-qPCR, EXPAR or RCA. Such techniques are therefore named homogeneous methods.

**3.2.1 Multiplex RT-qPCR.** One of the biggest RT-qPCR limitations lies in its multiplexing ability. The reverse transcription step can be performed simultaneously for all target miRNAs by using any of the RT strategies presented in Section 2.1, but the qPCR, however, can only be performed on a few miRNAs simultaneously. This is due to fluorescence emission spectra overlap that limits the number of fluorescence colors simultaneously distinguishable. In the best cases, multiplex qPCR is limited to six colors. Noteworthy, a 15-plex qPCR detection of 16S RNAs was performed by using different combinations of two spectrally distinct fluorophores out of six to identify bacterial species.<sup>100</sup> This strategy is not adapted however to the profiling of multiple RNA species present in the same sample, as multiple combinations of targets would generate the same signal, leading to a degeneracy issue. This problem can be solved mathematically by adjusting the probes concentrations so that the output signal corresponds only to one possible input combination.<sup>101</sup> To our knowledge, this strategy has not been implemented to increase the multiplexing capabilities of RT-qPCR in miRNA quantification. In addition, multiplying the number of primers increases the risk of primer dimer reaction and thus, requires careful design and tuning of the experimental conditions to guarantee specific amplification of all targets.

To circumvent this specificity issue, qPCR mix is typically diluted after one-pot reverse transcription, and distributed in 96- or 384-well plates, each well containing different miRNA-specific primers as well as universal primers and fluorescent probes.<sup>102</sup>

**3.2.2 Isothermal multiplex homogeneous assays.** Fluorescence is the most common readout for in-solution detection assays, but spectral overlap therefore limits their multiplexing capabilities.

Hildebrandt's group developed several amplification-free multiplex detection methods in solution, using either fluorescent dyes<sup>103</sup> or quantum dots (QD).<sup>104,105</sup> These methods use the miRNA to bring FRET donor and acceptor within close proximity either by ligation or base stacking. Interestingly, they reported the simultaneous detection of two miRNAs using a single FRET pair (terbium complex/QD), whose photoluminescence is tuned by the distance between the donor and the acceptor, reaching sub-nanomolar sensitivity. By coupling this temporal multiplexing

with enzyme-free amplification, the same team reported a gain in sensitivity of three orders of magnitude.<sup>106,107</sup> More recently, they combined spectral and temporal multiplexing to detect four DNA analogues of miRNAs with RCA.<sup>108</sup> Quantum dots were also used by Ye *et al.* in a 4-plex microfluidics-based assay.<sup>109</sup> RCA was also used by Wang *et al.* in a 3-plex assay displaying a LOD of 90 fM.<sup>110</sup>

Interestingly, the chromogenic cationic polymer poly[9,9-bis(60-*N,N,N,N*-trimethylammonium)-hexyl]-fluorenylene phenylene dibromide] (PFP) has been used as a universal FRET donor, allowing the detection of three miRNAs, combined with orthogonal fluorescent probes and DNAzyme-based amplification.<sup>111</sup>

Color-coded fluorescent reporters were also widely applied to amplified homogeneous detection methods, such as the first DSNSA miRNA multiplex detection by Yin and coworkers.<sup>76</sup> The LOD of the method (100 fM) was indeed improved compared to amplification-free techniques. Other DSN-based fluorescent methods were subsequently reported, most notably Xiao's 3-plex assay, using fluorescent probes embedded in MoS<sub>2</sub> nanosheets to improve specificity.<sup>80,112,113</sup>

**3.2.3 Fluorescence-based digital methods.** Fluorescence intensity level encoding is a possible way to perform multiplex detection past the “one target per color” barrier. In previously described fluorescence-based methods, however, signal intensity (referring either to an amplification time or a luminescent intensity) was used to compute the miRNA concentration. Additionally, these methods only provide relative quantification of their target requiring assay calibration with standard samples. Digital readout refers to methods where the absolute target concentration is directly computed from a ratio of positive (target-containing) and negative (empty) partitions, following the poissonian distribution of target molecules throughout these partitions. Digital PCR (dPCR) is undoubtedly the most widespread method for digital nucleic acid quantification. This method relies on the partitioning of the sample into microchambers<sup>114</sup> or microdroplets<sup>115</sup> (the latter referred as droplet digital PCR, ddPCR) thanks to microfluidics, in such a way that every partition contains either zero, one or a few cDNA or RNA molecules, according to the Poisson distribution. The RT step can either be performed before or after sample partitioning. Following thermocycling, the partitions are analyzed by imaging or in-line fluorescence readout. Absolute quantification of the cDNAs is achieved by counting the fluorescence-emitting (*i.e.* cDNA-containing) partitions and assuming the cDNA repartition followed a Poisson distribution. This quantification mode does not rely on fluorescence intensity, which is thus available for multiplexing. Introducing different probe concentrations, several groups managed to break the one target per color barrier for the detection of DNA molecules.<sup>116</sup>

Our group recently reported a multiplex isothermal amplification method using orthogonal EXPAR-like designs.<sup>117</sup> By solving the problem of cross-reactivity often observed in one-pot multiplex reactions, this work demonstrated a 3-plex assay using a droplet digital readout.

Smith *et al.* recently reported an ingenious use of RCA for single-molecule miRNA detection.<sup>118</sup> Following one-pot multiplex RCA, RCA products are labelled with probes tagged with

different fluorophores, which allows miRNA indexation. They achieved as a proof of concept a duplex miRNA detection with sub-pM sensitivity. The analysis was performed by single-molecule flow cytometry, as DNA molecules produced by RCA were large enough (48 kb) to be detected using conventional instruments. Although the authors only demonstrated a duplex detection as their proof of concept, it is clear that the barcoding capacity can reach hundreds or even thousands of combinations. The sensitivity of the assay, however, still needs to be improved to match the requirements of miRNA profiling in biological samples. This may be caused by non-specific initiation of RCA, which could be reduced by using padlock probes.<sup>119</sup> Hu and coworkers however reported a similar method using padlock probes displaying similar sensitivity (1 pM).<sup>120</sup> One can note the development of a similar strategy applied to multiplex nucleic acid detection, combined with a microfluidic-driven enrichment step to improve the sensitivity.<sup>121</sup>

**3.2.4 Next generation sequencing.** Next generation sequencing (NGS) is an emerging technology for miRNA profiling. In order to perform RNA sequencing (RNA-seq), the RNAs of the sample first need to be extracted and purified. After purification, universal adapters are ligated, typically to the 5' and 3' ends of each RNA strand (alternatively, a single adapter can be ligated to the 3' end followed by circularization of the product<sup>122</sup>). A reverse-transcription step is then performed, followed by a PCR amplification and finally, sequencing.

NGS historically allowed the discovery of a plethora of miRNAs,<sup>123</sup> as NGS instruments are able to read millions to billions of sequences in a few days. This very high throughput is one of the advantages of NGS, and is extremely important for miRNA profiling. NGS is indeed the miRNA detection method that displays the highest multiplexing ability, since all RNAs in the sample can theoretically be detected, thanks to the use of universal RT and PCR primers.<sup>124</sup> RNA-seq thus requires no prior information or specified target sequence. This ability makes RNA-seq unique among miRNA detection methods, because most other techniques require the design of specific primers and/or probes for each targeted miRNA, which reduces the spectrum of the analysis. The specificity of NGS miRNA detection depends on the error rate of the sequencing platforms, which is typically around 1–10 errors for 1000 bases called.<sup>125</sup> Since miRNAs are around 20 bases long, NGS is very accurate for the differentiation of miRNAs, even highly homologous sequences.

While it displays undeniable advantages, NGS still suffers from several flaws. Owing to its lack of sensitivity, sequencing analysis always requires a pre-amplification step traditionally achieved by RT-qPCR (which also converts the RNA sequence into DNA material readable by DNA sequencing). The reverse-transcription and PCR steps can generate sequence-dependent biases,<sup>126,127</sup> making this technique poorly quantitative. Additionally, rare sequences are often dropped out because of abundant RNAs drawing most of the reads, thus reducing the sensitivity. NGS equipments are still very expensive, which makes, so far, routine diagnosis impossible. Each analysis provides a great amount of useful information, the extraction of which requires time and skilled bioinformaticians.



In spite of its drawbacks, comprehensive miRNA analysis by NGS is progressively becoming a benchmark to identify disease-linked miRNA signatures.<sup>128,129</sup> Coenen-Stass *et al.*, for example, reported a dysregulated miRNA profile for the diagnosis of Duchenne muscular dystrophy using NGS.<sup>130</sup>

### 3.3 Heterogeneous multiplex detection

**3.3.1 On-sensor methods.** Several readout strategies can only be performed on a surface, forbidding their use in fully in-solution – homogeneous – format. On-sensor methods refer to the use of a surface to perform the readout, coupled to orthogonal signals for multiplexing (as opposed to microarrays that use universal reporting for all targets, combined with spatial indexation, see Section 3.3.3.1). This is the case for electrochemical readout, since electrodes are needed to measure the intensity in the solution.

This method has been applied to multiplex miRNA detection in a planar format by Yuan's group. The team first coupled electrochemical readout to DSNSA, achieving detection limits of a few fM.<sup>131</sup> The sensitivity was further improved to reach a LOD around 50 aM by designing a DNA bot triggering the degradation of electrochemical labels upon miRNA capture.<sup>132</sup> The group so far demonstrated the simultaneous detection of two targets using methylene blue and ferrocene as electro-labels. Xu and coworkers reported a LOD of 20 aM for a similar assay relying on a DNA framework changing conformation upon miRNA capture.<sup>133</sup>

Similar designs were developed in suspension, using the target miRNA to modify the distance between a magnetic microparticle and a miRNA-specific electrolabel.<sup>134–136</sup> To our knowledge, all of the so far reported electrochemical on-particle methods demonstrated a duplex miRNA detection. The most sensitive of those methods reported a limit of detection around 1 fM.<sup>135</sup>

In all aforementioned electrochemical assays, each target is quantified using a different electrochemical label. As for fluorescence-based homogeneous assays, the multiplex ability of this method is limited by the number of electrochemical dyes simultaneously distinguishable by square wave voltammetry. Alternatively, mass spectrometry has demonstrated a high multiplexing potential using dozens of orthogonal metal isotopes.<sup>137</sup> Such readout was for example combined with lanthanide-tagged recognition probes and DSNSA in a triplex assay.<sup>138</sup>

Surface-enhanced Raman scattering (SERS) is a powerful technique allowing the enhancement of Raman light scattering signals by up to 11 orders of magnitude.<sup>139</sup> The method requires the interaction of two surfaces brought within close proximity to amplify the signal, and is therefore a heterogeneous-only detection method. SERS can for example be applied to sandwich assays using Raman-barcoded particles.<sup>140,141</sup> Su *et al.* designed SERS “nano-mushrooms”,<sup>140</sup> composed of a gold core linked to a silver cap by DNA spacers. The gap between the gold and silver surfaces forms a signal-enhancing “hotspot”, in which Raman labels are inserted. The gold core of the mushroom is coupled to DNA probes specific to one miRNA target, and are accordingly barcoded by inserting different Raman dyes in the hotspot. In

this assay, the miRNA forms a bridge between a magnetic microparticle and its specific SERS nano-mushroom. After hybridization, the microparticles are recovered and each target is quantified by measuring the intensity of the corresponding Raman signals. The authors demonstrated a 3-plex assay with a 1 pM detection limit. Zhou and coworkers increased the sensitivity by a 100-fold by using gold-Raman Nanobridge Nanogap Probes (Au-RNNP).<sup>141</sup> Instead of a sandwich detection, Wang *et al.* designed the “Inverse Molecular Sentinel” (IMS) assay.<sup>142</sup> They used gold particles specifically engineered for signal enhancement, called Nanostars. Raman-labeled hairpins were immobilized on the particles. In the absence of the miRNA, the hairpins are opened and partially hybridized to the miRNA capture probe. The miRNA is perfectly complementary to its capture probe and can hybridize to it, strand-displacing the hairpin in the process. The hairpin then closes, bringing the Raman dye close to the SERS-inducing tips of the Nanostar particle, which amplifies the Raman signal of the dye. This technique enabled the duplex detection of miRNAs from total RNA cell extracts.

While most of the herein presented SERS-based assays rely on the use of Raman dyes, Sim's group developed a label-free miRNA detection method, able to recognize the Raman signature of the miRNA directly.<sup>143</sup> Although the label-free approach reduced the sensitivity (5 fM) compared to other assays from the same group (Section 3.3.3, planar microarrays), the multiplexing potential of the method appears promising.

**3.3.2 Nanostring.** The NanoString nCounter system is an emerging technology for multiplexed miRNA detection. It was originally developed for gene expression monitoring by quantifying messenger RNAs<sup>144–146</sup> and adapted for miRNA detection.<sup>147,148</sup> This system allows single-molecule detection using a microarray-inspired principle. As for a classical microarray, the miRNA hybridizes to a capture probe and a detection probe (Fig. 10). The capture probe, 35 to 50 base-long and coupled to biotin on its 3' end, binds the 5' half of the miRNA. The detection probe is composed of a 3' end complementary to the miRNA and a chain of fluorescently labeled RNA sequences, forming a fluorescent

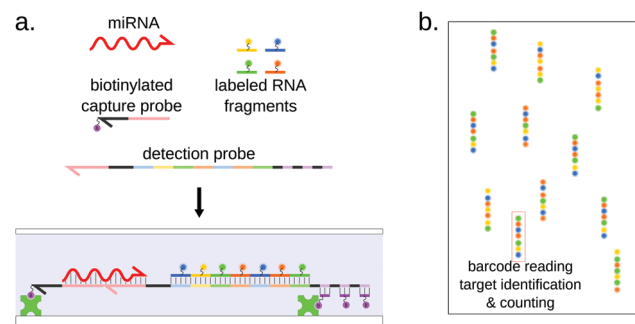


Fig. 10 Principle of the Nanostring nCounter system. (a) The miRNA bridges between biotinylated capture probe, allowing immobilization on a glass slide, and a detection probe carrying a combination of fluorescent labels allowing identification of the target miRNA. (b) The immobilized sets of labels are counted, each one of them reporting the capture of a single miRNA molecule.



barcode associated with the target miRNA. After hybridization of both probes, the complex is immobilized on a surface thanks to the biotin tag on the capture probe, and fluorescence imaging is performed. Analysis consists simply in counting fluorescent barcodes, each of them indicating the capture of one miRNA molecule.

This single-molecule approach grants the nCounter system with great sensitivity, in the sub-fM range,<sup>144</sup> without requiring any amplification. This technology still displays some limitations in terms of specificity and assay duration.<sup>45,148</sup>

The multiplexing ability of the nCounter system lies in the fluorescently barcoded RNA fragments on the reporter probe. They are prepared separately by incorporating amino-allyl-modified UTPs during transcription of the fragments and coupling the modified uracil residues to four different dyes.<sup>144</sup> The reporter probe is then assembled from a template by ligating seven fluorescent RNA fragments and the miRNA-specific 5' end together. This strategy of seven fluorescent RNAs, with four possible colors for each of them, allows more than 15 000 possible combinations. Taking into account that two consecutive fragments must be of different colors, the number of combinations is still 2916, while only 2654 miRNA sequences are referenced for *Homo Sapiens* in miRbase.<sup>149</sup> In practice, Nanostring proposes detection panels of up to 800 human miRNAs. This effective barcoding strategy places this technology among the highest multiplexing methods, in the same range as density-based microarrays, while supposedly outperforming them in terms of sensitivity and sample requirement thanks to single-molecule counting.<sup>144</sup> This statement is however contradicted by a study by Mestdagh *et al.*,<sup>45</sup> where the authors benchmarked 3 microarray platforms (including Agilent, Affimetrix and Nanostring) and concluded that the nCounter system did not display higher sensitivity and was even poorly performing with low-input amount of RNA. The nCounter system was recently used to screen for possible cancer miRNA signatures, for example in breast<sup>150</sup> and ovarian<sup>151</sup> cancers.

**3.3.3 Microarrays.** Microarrays are detection methods enabling multiplexing by spatially separating the specific receptors of each target. These methods can be divided into two main categories: planar arrays and suspension (*i.e.* on-particle) arrays. In suspension arrays, each particle is coupled to capture probes for a single analyte and is given a corresponding “barcode”, indicating what is the target of the particle. Given the diversity of available particles, various barcoding strategies were implemented, such as size, graphical and most commonly fluorescence encoding. Planar arrays, or flat-arrays, use spatial separation as a multiplexing strategy: specific capture probes are spotted on a flat surface, each spot targeting a different analyte. Both approaches display interesting characteristics, especially in terms of multiplexing.

**3.3.3.1 Planar microarrays.** Planar arrays are composed of high-density spots of DNA probes immobilized on a flat glass or polymer support<sup>152</sup> (Fig. 11). These probes can capture one specific target by Watson–Crick base-pairing. Each spot comprises only one kind of DNA capture probes, and can in theory only capture one kind of target. The sample is flown on

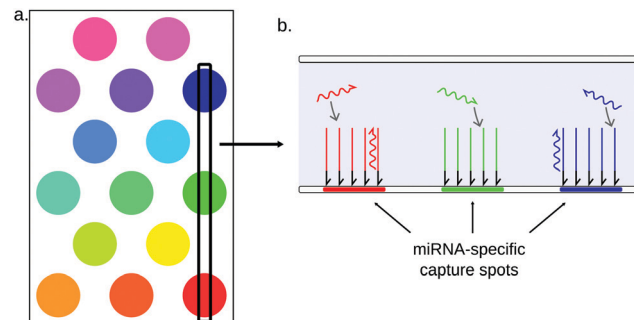


Fig. 11 Principle of planar microarrays. (a) Capture probes are immobilized on a surface, forming separated spots. (b) Each spot is exclusively composed of capture probes for the same miRNA. Multiple readout strategies can be employed to quantify the miRNAs.

the support, and every target sequence is captured on its specific probe spot. Multiple targets can thus be simultaneously quantified by measuring the signal on each spot. The spatial target separation allows microarrays to detect up to hundreds to thousands of nucleic acid sequences simultaneously [Yin, 2008]. Thanks to this excellent multiplexing ability, microarrays are often used for miRNA screening assays, leading for example to the identification of disease miRNA signatures.<sup>153,154</sup>

Most conventional microarrays require the enrichment and labelling of potential targets prior to hybridization. In the case of miRNAs, the enrichment step consists in the separation of short RNAs (usually under 200 nt) from total RNA. All short RNAs are then labelled, typically using radioactive or fluorescent labels.<sup>155</sup> The labelling can be performed either directly on the RNA strands, by ligating a fluorescent dye<sup>156,157</sup> or a biotin residue<sup>158</sup> to one of the miRNA ends, or indirectly following a reverse-transcription step<sup>159</sup> and possibly a PCR amplification.<sup>160,161</sup>

Despite being high-throughput and highly multiplexed, classic miRNAs microarrays display a relatively low sensitivity, with detection limits within the nanomolar range. Moreover, since the yield of labelling, enrichment and/or amplification steps often varies depending on the sequence, these steps can introduce quantification biases. The hybridization step is also prone to biases due to the variable miRNA hybridization thermodynamics.<sup>162</sup> The specificity of conventional microarrays is also relatively low towards highly homologous miRNAs, which requires long hybridization steps (up to several days). The implementation of LNA-modified<sup>163</sup> or stem-loop capture probes<sup>164</sup> is reported to improve the specificity.

The relatively low sensitivity of conventional microarrays is a critical issue for the detection of low-abundant miRNAs in real samples. In order to detect lower concentrations, two main options are available: improving the sensitivity of the detector, or increasing the target concentration. In this section, we will focus on new detectors and readout strategies applied to the detection of miRNAs.

As was already presented, SERS is a very powerful surface-based signal amplification technique. Sim's group for example reported significant advances for SERS-based multiplex miRNA



detection.<sup>143,165</sup> The group designed a sensor composed of gold nanopillars, the tips of which are coupled to miRNA-specific DNA capture probes. The sensor allowed the sensitive detection of 3 miRNAs simultaneously, either by amplifying the Raman signal of the miRNA itself<sup>143</sup> or in a labeled sandwich assay format.<sup>165</sup> The assays are indeed more sensitive than conventional microarrays: the LOD of the direct detection method is a few fM, and the sandwich assay can even detect concentrations in the attomolar range, with a 9 orders of magnitude dynamic range. Liu *et al.* also designed a SERS-based microarray.<sup>166</sup> The method uses Raman-labeled nanoparticles that compete with miRNA to bind miRNA-specific capture probes coupled to the sensor. The concentration of target miRNA for each spot is thus inversely related to the intensity of the Raman signal. Interestingly, the proof of concept assay was an 8-plex detection of the members of the Let7 family, showing the excellent specificity of the method. The LOD was around 100 fM, not as good as previously reported nanopillar-based methods.

Other reporting strategies for amplification-free miRNA sensing were developed, such as surface-plasmon resonance,<sup>167,168</sup> microring resonators,<sup>169</sup> electrochemistry<sup>170,171</sup> or gold nanoparticles aggregation.<sup>172</sup> None of these technologies have however surpassed SERS in terms of sensitivity.

The high multiplexing ability of microarrays can also be used to enhance the potential of conventional techniques, such as RT-qPCR<sup>173,174</sup> or LAMP.<sup>175</sup> Choi *et al.* for example proposed an on-support version of RT-qPCR.<sup>173</sup> In this method, following the RT step, the cDNA mix is introduced in a microfluidic channel. Hydrogel microposts were formed in the middle of the microchannel. The microposts are photochemically coupled to miRNA-specific PCR primers, allowing each post to capture its specific cDNAs. Quantitative PCR is performed using a universal reverse primer in solution, and amplification is reported by SYBR Green I fluorescence. Although less sensitive than in-solution RT-qPCR, this assay displays increased multiplex potential, because the independent PCR amplifications are spatially separated, mitigating cross-reactivity issues. A similar assay using LAMP amplification coupled to an electrochemical readout was developed by Hashimoto and coworkers.<sup>175</sup> A 5-plex detection with a LOD in the 100 aM range was demonstrated. Alternatively, Ishihara *et al.* used a dendritic amplification step by flowing fluorescent streptavidin and biotinylated anti-streptavidin antibodies.<sup>176</sup> Instead of capturing the target and then amplifying the signal, the other approach is to perform an amplification in solution prior to capturing and labeling the amplified target. Mader *et al.* performed a 14-plex detection based on nucleic acids sequence-based amplification (NASBA) using this approach.<sup>177</sup>

**3.3.4 Suspension arrays.** The fundamental difference between planar and suspension microarrays is the mobility of detection particles. Instead of being tethered on a surface, analyte receptors are therefore spread throughout the entire volume.<sup>178</sup> As both targets and capture probes diffuse in the sample, the analyte–receptor encounter probability is increased, resulting in faster capture kinetics. This feature is of crucial importance given the duration of hybridization protocols for planar microarrays (up to several days).

One of the main challenges for multiplexed detection is that several output signals not only need to be measured, but also attributed to the corresponding target. For homogeneous methods, target identification is mostly based on two strategies: the use of different fluorescent reporters or the coupling to separative techniques. In the case of planar arrays, the indexation is encoded in spatially distinct spots. Barcoding designates the various indexation methods for suspension microarrays. Thanks to the diversity and versatility of particles and functionalization techniques, the field of suspension arrays offers a greater variety of barcoding strategies and shows excellent multiplexing potential.

**3.3.4.1 Fluorescence.** As for homogeneous assays, fluorescence is the most common barcoding strategy for particle-based methods. In this case, it is however possible to surpass the typical limitation of six colors by encoding the particles with different intensities for a single fluorescent channel.

Fluorescently barcoded particles can be prepared using various techniques. The easiest of them is the functionalization of the surface of the particle with fluorescent oligonucleotides, either using affinity or covalent coupling.<sup>179</sup> Alternatively, dyes can be integrated to the core of the particle, in the form of dyes<sup>180</sup> or Quantum Dots (QD) (Fig. 12).<sup>181,182</sup>

The Luminex xMAP system is a commercial set of more than 100 fluorescent microparticles subpopulations, widely used for multiplex detection assays. Li *et al.* applied this system for the amplification-free detection of 4 miRNAs in a single assay.<sup>183</sup> The technique displayed a relatively high detection limit (500 fM). Causa and coworkers notably reported another amplification-free 3-plex method using fluorescent hydrogel particles, displaying remarkable sensitivity for such assays, in the fM range.<sup>180</sup> A similar limit of detection was achieved by Tao's group.<sup>184</sup> Additionally, the authors managed to break the “one target per color” barrier by relying on particle colocalization for reporting: 6 miRNAs were simultaneously detected using only 4 fluorescent particles populations.

Fluorescent particles are also compatible with amplification techniques, such as DSNSA,<sup>182</sup> strand-displacement

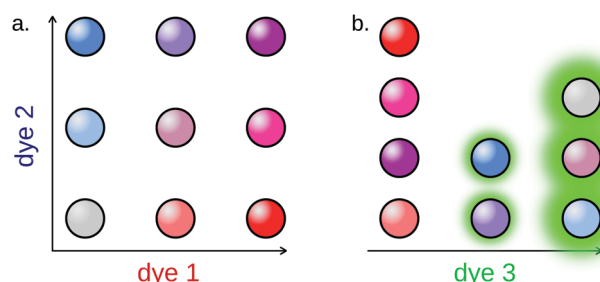


Fig. 12 Example of fluorescent particle barcoding. (a) Fluorescent particle barcoding allows to overcome the “one color per target” barrier by combining intensity levels of fluorophores. In this example, using 2 dyes, each of which can be introduced in 3 distinct intensity levels, allows the barcoding of up to  $3^2 = 9$  subpopulations. (b) Reporting is performed using an independent fluorescence channel, the intensity of which can be used to compute the miRNA concentration.



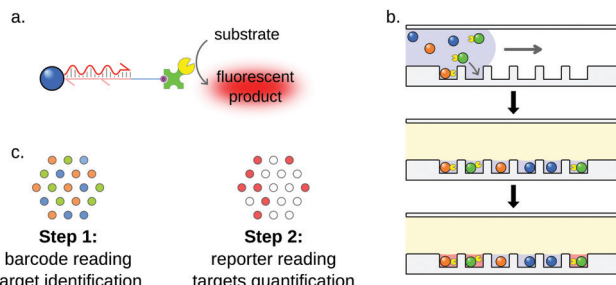


Fig. 13 Principle of the SIMOA detection system. (a) The hybridization of the miRNA to its specific capture probes allows the capture of  $\beta$ -galactosidase on a barcoded microparticle. (b) Simplified workflow. After enzyme capture, particles are trapped in individual microwells and incubated. (c) Readout is performed in two steps. First, particle barcodes are read, enabling target identification. Then, reporter fluorescence is measured, indicating whether the targeted miRNA was captured or not. Since the capture of miRNAs by particles follows a Poisson distribution, absolute quantification of the target can be achieved by simply counting "ON" and "OFF" wells for each miRNA.

amplification<sup>105</sup> or SIMOA detection. The single molecule array (SIMOA) is a suspension array designed by Quanterix corporation. This system allows the detection of analytes down to the single-molecule level thanks to microfluidics.<sup>185,186</sup> Originally developed for the detection of proteins,<sup>185,187,188</sup> the assay was later adapted to digital nucleic acid detection (Fig. 13).<sup>189</sup> In this technology, microparticles are functionalized with miRNA-specific capture probes. The target miRNA is used to bridge the capture probe and a reporter oligonucleotide tagged with a beta-galactosidase. The particles are then isolated in individual wells carved on a microfluidic chip. The hydrolysis of a fluorogenic substrate by the beta-galactosidase reports the capture of the target in each well. Fluorescent imaging of the microfluidic chamber, followed by poissonian analysis allows the absolute quantification of the target. Cohen *et al.* reported a 3-plex digital detection of miRNAs using the SIMOA system.<sup>179</sup> The assay showed good sensitivity, as the limit of detection was approximately 10 fM. In order to improve the specificity of the multiplex detection, LNA capture probes were designed, which prevented any cross-reactivity between the three targets. The method was further validated by a comparison with gold-standard RT-qPCR, showing convincing results even from total RNA cell extracts.

**3.3.4.2 Graphical barcoding.** Graphical barcoding consists in shaping or engraving visual patterns in order to differentiate beads subpopulations. This strategy allows for highly multiplexed assays, as the pool of potential symbols or patterns that can be encoded in the particles is only limited by patterning resolution.<sup>190</sup> Doyle's group extensively used such encoded particles for multiplexed miRNA detection.<sup>191–193</sup> Their hydrogel particles are barcoded by a set of five length-coded stripes, using stop-flow lithography. As there are three possible lengths for each stripe, there are  $3^5 = 243$  possible combinations. The authors demonstrated the potential of these particles for miRNA detection in real samples, such as formalin-fixed paraffin-embedded tissue<sup>192</sup> or raw cell lysates.<sup>193</sup> The

introduction of a RCA amplification step increased the sensitivity of the assay by 100-fold.<sup>191</sup> The same group also designed polygon-shaped, easily recognizable particles for mobile phone readout.<sup>194</sup> Doyle's group also designed digital patterns, with a set of 8 spots, each of them being in a 0 (no engraving) or 1 (engraved) state, for a similar capacity (256 combinations).<sup>195</sup> As a proof of concept, the authors demonstrated a multiplex assay where barcoded hydrogel particles targeting 3 different miRNAs are individually trapped in a microfluidic chamber prior to an enzymatic ( $\beta$ -galactosidase) signal amplification, achieving a 10 fM limit of detection. A similar digital encoding was used by Liu on silica particles, reaching 128 possible subpopulations and demonstrating a duplex assay.<sup>196</sup> The experimental design included a RCA step to improve sensitivity, reaching 1 fM. Jung and co-workers reached an exceptional  $3^{12}$  combinations with radially-encoded polyethylene glycol half-spheres, which they used in combination with qPCR-based detection method.<sup>190</sup> MiRNA-specific primers are chemically grafted in the gel matrix, and the particles are graphically encoded by lithography. Following a common RT step, cDNAs are specifically captured by the immobilized primers, inside the pores of the corresponding particle. RT-qPCR is then performed using universal reverse primers in solution. After each cycle, the fluorescence of each particle is measured by microscopy. The method allowed to perform a 10-plex detection from purified extracellular vesicles. The sensitivity of the assay was significantly reduced (1 pM) compared to conventional RT-qPCR. The authors report that the specificity of this supported qPCR is superior to that of solution qPCR. In spite of this exceptional multiplexing ability, such techniques are neither as easy, nor as commonly used as fluorescence barcoding strategies, possibly because of the need for special equipment and expertise for generating the particles (Fig. 14).

**3.3.4.3 Photonic crystals.** A photonic band-gap crystal, or photonic crystal (PhC), is a spatially periodic structure composed of materials having different dielectric constants.<sup>197</sup> In such structures, photons of a chosen wavelength can not propagate and are therefore reflected, whereas all other wavelengths are transmitted. The excluded wavelength, or bandgap, depends on dielectric constants of the materials and on the characteristics of the periodic lattice itself. The reflected wavelength range is thus highly tunable. The advantages of using photonic crystals as particle barcodes are numerous: PhCs are highly stable and are not affected by photobleaching. Being a fluorescence-free strategy, photonic crystal particles do not interfere with fluorescent reporting.<sup>198–200</sup> Contrary to fluorescence barcoding, photonic crystal particles cannot be intensity-encoded. Moreover, the reflection spectra of PhCs are Gaussian peaks with a typical half-height width of 25 nm,<sup>199</sup> which limits the number of simultaneously distinguishable populations, just like overlapping emission spectra do for fluorescence barcoding. The preparation of such particles is also a limitation, as it is very expertise-demanding. These drawbacks may explain why, in



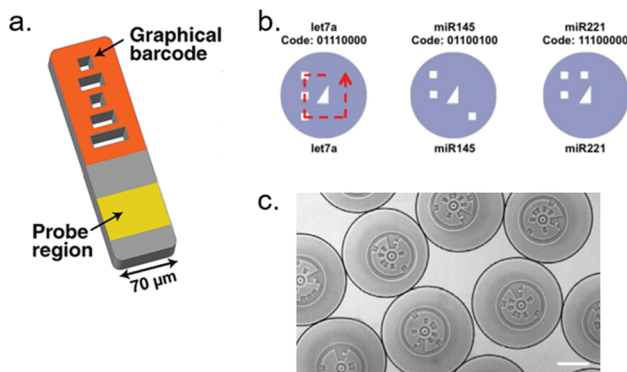


**Fig. 14** Examples of graphical particle barcoding. (a) Hydrogel particle encoded by 5 stripes of various lengths. Picture extracted from Chapin and Doyle.<sup>191</sup> (b) Example of digital encryption: each particle presents 8 spots that can be engraved (1 state) or not (0 state). The central triangle is used for orientation. Picture from Kim *et al.*<sup>195</sup> (c) Each particle carries a circular barcode divided in 16 angular sectors. Picture from Jung *et al.*<sup>190</sup>

spite of their attractive qualities, PhC particles are still an uncommon barcoding strategy (Fig. 15).

The use of PhC particles for multiplexed miRNA detection was demonstrated by Zhao's group, either coupled to RCA<sup>199</sup> or HCR.<sup>198,200</sup> The highest sensitivity was obtained using a RCA step, with a LOD of 20 fM. All designs allowed the detection of up to 3 miRNAs simultaneously. Due to overlapping reflection spectra, the maximum multiplicity of PhCs appears to be 5 subpopulations.

**3.3.4.4 Size encoding.** Particle size encoding is an easy way for subpopulations barcoding. Size-coded particles can simply be differentiated by microscopy, or flow cytometry by measuring particles forward light scattering (FSC).<sup>201,202</sup> Particles of different sizes but similar densities can also be distinguished based on their mass, using separative techniques such as field-flow fractionation (FFF)<sup>203</sup> or acoustic levitation.<sup>204</sup> Size-based

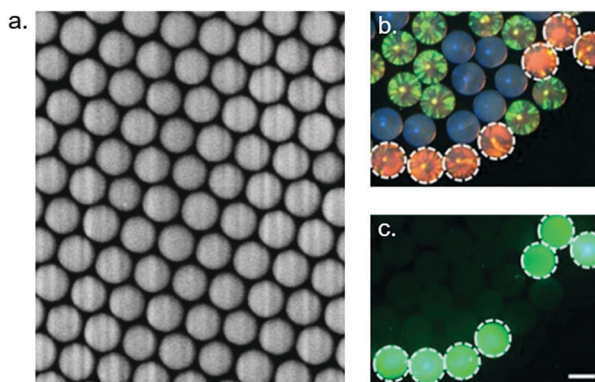


**Fig. 15** Photonic crystal particles. (a) Electron microscopy image of the surface of a photonic crystal particle. (b) Reflection images of photonic particles with blue, green and red structural colors. (c) Fluorescence image of the particles shown on (b). Green fluorescence intensity allows quantification of the corresponding target. White light reflection by the photonic crystal and fluorescence emission are completely independent. Pictures from Bian *et al.*<sup>198</sup>

barcoding is however a relatively uncommon strategy, mostly because of its low multiplexing potential, as none of the aforementioned techniques can detect subtle size variations. To our knowledge, the highest demonstrated multiplex miRNA detection using size-coded particles was a 4-plex assay by Wang *et al.*<sup>202</sup>

Although size coding may not be easily scalable, the main quality of this method is its compatibility with other barcoding strategies. The combination of fluorescent barcoding with an additional size-based encryption level appears as particularly promising: both approaches can easily be combined, as affinity tag-coated particles of various sizes are widely available. Moreover, both particle size and fluorescence can be measured simultaneously by flow cytometry, which makes this multimodal strategy particularly convenient.

**3.3.4.5 Other barcoding strategies.** Among the numerous suspension-based methods for multiplexed miRNA detection, Kim and coworkers proposed a unique barcoding strategy.<sup>205</sup> Their approach is based on three encryption levels: first, they used plasmonic nanoparticles as detection particles. The three different kinds of particles (gold–silver nanorods, gold nanospheres and silver nanospheres) had different light-scattering

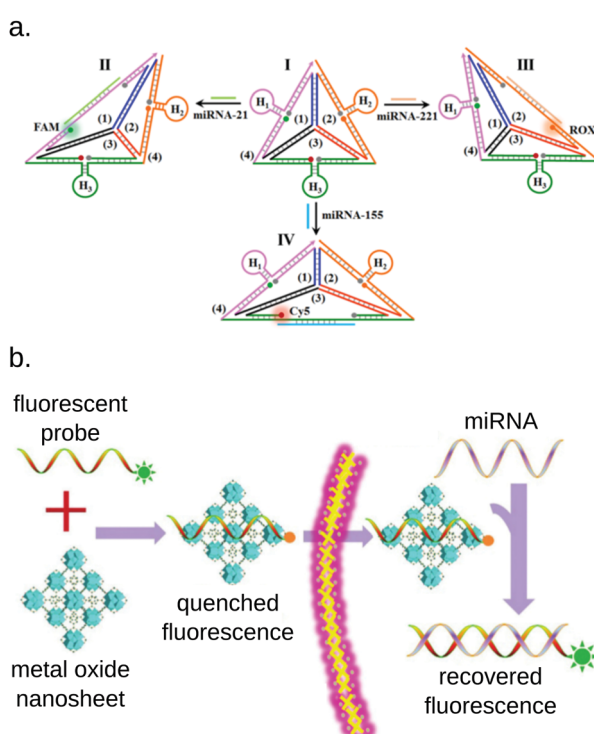


**Fig. 16** Examples of common approaches for miRNA detection from live cells. (a) DNA framework allowing the simultaneous of 3 miRNAs simultaneously. All 3 fluorophores are initially quenched. The binding of a miRNA changes the conformation of the framework, taking the corresponding fluorophore and its quencher apart. Picture from Zhou *et al.*<sup>213</sup> (b) MiRNA detection based on metal oxide nanosheets. The fluorescent probes are initially embedded in the nanosheet, which quenches their fluorescence. Upon miRNA hybridization, the probe is freed from the nanosheet, and fluorescence is recovered. Picture from Wu *et al.*<sup>209</sup>

**Table 1** Summary of the characteristics of the discussed multiplex miRNA detection methods. Asterisks indicate that the limit of detection was calculated by adding 3 standard deviations to the average blank. Non-asterisk references did not indicate how the LOD was calculated. Please note that the specificity criterium is not included in the table as it is often partially or not assessed in the listed references

Type	Amplification	LOD	Readout	Target indexation	Highest multiplex	Ref.
Homogeneous	HCR	25 amol	NB	Fluorescent dye	3	Schwarzkopf <i>et al.</i> <sup>86</sup>
Homogeneous	Ligation PCR	1 pM	PAGE	Size separation	9	Arefian <i>et al.</i> <sup>93</sup>
Homogeneous	No	130 fM	Agarose gel	Conformation separation	5	Chandrasekaran <i>et al.</i> <sup>94</sup>
Homogeneous	No	190 fM*	CE	Size separation	5	Jiang <i>et al.</i> <sup>95</sup>
Homogeneous	Ligation PCR	200 aM	CE	Size separation	5	Zhang <i>et al.</i> <sup>96</sup>
Homogeneous	EXPAR	2 fmol	CE	Conformation separation	8	Na <i>et al.</i> <sup>98</sup>
Homogeneous	DSNSA	260 aM	HPLC	Size separation	3	Qi <i>et al.</i> <sup>99</sup>
Homogeneous	No	200 pM*	Fluorescence	Fluorescent dye	3	Jin <i>et al.</i> <sup>103</sup>
Homogeneous	No	40 pM*	Fluorescence	Fluorescent dye	3	Qiu <i>et al.</i> <sup>104</sup>
Homogeneous	No	500 pM*	Fluorescence	FRET decay time	2	Qiu <i>et al.</i> <sup>105</sup>
Homogeneous	No	40 pM	Fluorescence	Fluorescent dye	4	Ye <i>et al.</i> <sup>109</sup>
Homogeneous	RCA	90 fM*	Fluorescence	Fluorescent dye	3	Wang <i>et al.</i> <sup>110</sup>
Homogeneous	HCR	0.88 pM*	Fluorescence	FRET decay time	2	Guo <i>et al.</i> <sup>106</sup>
Homogeneous	CHA	1.8 pM*	Fluorescence	FRET decay time	2	Xu <i>et al.</i> <sup>107</sup>
Homogeneous	RCA	0.3 fM*	Fluorescence	FRET dye and decay time	4	Qiu <i>et al.</i> <sup>108</sup>
Homogeneous	DNAzyme	15 fM	Fluorescence	Fluorescent dye	3	Tang <i>et al.</i> <sup>111</sup>
Homogeneous	DSNSA	100 fM*	Fluorescence	Fluorescent dye	3	Yin <i>et al.</i> <sup>76</sup>
Homogeneous	DSNSA	9 pM*	Fluorescence	Fluorescent dye	3	Cui <i>et al.</i> <sup>112</sup>
Homogeneous	DSNSA	0.8 pM*	Fluorescence	Fluorescent dye	2	Liu <i>et al.</i> <sup>137</sup>
Homogeneous	DSNSA	10 fM*	Fluorescence	Fluorescent dye	3	Xiao <i>et al.</i> <sup>113</sup>
Homogeneous	EXPAR-like	10 fM	Fluorescence (digital)	Fluorescent dye	3	Rondelez and Gines <sup>117</sup>
Homogeneous	RCA	47 fM*	Flow cytometry	Combination of dyes	2	Smith <i>et al.</i> <sup>118</sup>
Homogeneous	RCA	1 pM*	Flow cytometry	Combination of dyes	3	Hu <i>et al.</i> <sup>120</sup>
On-sensor	DSNSA*	3 fmol	Voltammetry	Electrolabels	2	Yang <i>et al.</i> <sup>131</sup>
On-sensor	DNAzyme	50 aM*	Voltammetry	Electrolabels	2	Chang <i>et al.</i> <sup>132</sup>
On-sensor	No	20 aM	Voltammetry	Electrolabels	2	Xu <i>et al.</i> <sup>133</sup>
On-sensor	No	50 fM*	Voltammetry	Electrolabels	2	Zhu <i>et al.</i> <sup>134</sup>
On-sensor	No	0.2 fM	Voltammetry	Electrolabels	2	Wang <i>et al.</i> <sup>135</sup>
On-sensor	No	0.3 pM*	Voltammetry	Electrolabels	2	Azzouzi <i>et al.</i> <sup>136</sup>
On-sensor	DSNSA	58 fmol*	MS	Lanthanide tags	3	Zhang <i>et al.</i> <sup>138</sup>
On-sensor	No	1 pM	SERS	Raman labels	3	Su <i>et al.</i> <sup>140</sup>
On-sensor	No	10 fM*	SERS	Raman labels	3	Zhou <i>et al.</i> <sup>141</sup>
On-sensor	No	N/A	SERS	Raman labels	2	Wang <i>et al.</i> <sup>142</sup>
On-sensor	No	2 fM*	Raman spectrometry	miRNA Raman signature	3	Kim <i>et al.</i> <sup>143</sup>
Microarray (plan.)	No	1 aM	SERS	Spatial	3	Lee <i>et al.</i> <sup>165</sup>
Microarray (plan.)	No	200 fM*	SERS	Spatial	8	Liu <i>et al.</i> <sup>166</sup>
Microarray (plan.)	No	500* fM	SPR	Spatial	4	Sguassero <i>et al.</i> <sup>167</sup>
Microarray (plan.)	No	30 fM	SPR	Spatial	3	Yeung <i>et al.</i> <sup>168</sup>
Microarray (plan.)	No	10 pM	Microring resonator	Spatial	4	Qavi <i>et al.</i> <sup>169</sup>
Microarray (plan.)	No	<1 pM	Electrochemical	Spatial	8	Hofmann <i>et al.</i> <sup>170</sup>
Microarray (plan.)	Trapped enzyme	1 aM*	Electrochemical	Spatial	3	Wen <i>et al.</i> <sup>171</sup>
Microarray (plan.)	No	260 fM*	Au NP aggregation	Spatial	3	Lee <i>et al.</i> <sup>172</sup>
Microarray (plan.)	RT-qPCR	10 pg $\mu$ L <sup>-1</sup>	Fluorescence	Spatial	5	Choi <i>et al.</i> <sup>173</sup>
Microarray (plan.)	RT-qPCR	2 amol	Fluorescence	Spatial	5	Jung <i>et al.</i> <sup>174</sup>
Microarray (plan.)	LAMP	20 copies per $\mu$ L	Voltammetry	Spatial	5	Hashimoto <i>et al.</i> <sup>175</sup>
Microarray (plan.)	Dendritic	50 fM	Fluorescence	Spatial	3	Ishihara <i>et al.</i> <sup>226</sup>
Microarray (plan.)	DSNSA	N/A	Fluorescence	Spatial	14	Mader <i>et al.</i> <sup>177</sup>
Microarray (susp.)	SIMOA	1 fM*	Fluorescence	Fluorescent barcodes	3	Cohen <i>et al.</i> <sup>179</sup>
Microarray (susp.)	No	1 fM	Fluorescence	Fluorescent barcodes	3	Causa <i>et al.</i> <sup>180</sup>
Microarray (susp.)	Strand displacement	400 aM	Fluorescence	Fluorescent barcodes	3	Qu <i>et al.</i> <sup>181</sup>
Microarray (susp.)	No	500 fM	Fluorescent	Fluorescent barcodes	4	Li <i>et al.</i> <sup>183</sup>
Microarray (susp.)	No	1 fM*	Particle colocalization	Fluorescent barcodes	6	Tao <i>et al.</i> <sup>184</sup>
Microarray (susp.)	DSNSA	0.5 pM	Fluorescence	Fluorescent barcodes	2	Wang <i>et al.</i> <sup>227</sup>
Microarray (susp.)	RT-qPCR	100 fM	Fluorescence	Graphical barcodes	5	Jung <i>et al.</i> <sup>190</sup>
Microarray (susp.)	RCA	300 aM*	Fluorescence	Graphical barcodes	3	Chapin and Doyle <sup>191</sup>
Microarray (susp.)	Trapped enzyme	4 pM*	Colorimetry	Graphical barcodes	3	Juthani and Doyle <sup>194</sup>
Microarray (susp.)	No	2 amol*	Fluorescence	Graphical barcodes	5	Lee <i>et al.</i> <sup>192</sup>
Microarray (susp.)	No	2 amol*	Fluorescence	Graphical barcodes	5	Nagarajan <i>et al.</i> <sup>193</sup>
Microarray (susp.)	Trapped enzyme	60 zmol*	Fluorescence	Graphical barcodes	3	Kim <i>et al.</i> <sup>195</sup>
Microarray (susp.)	RCA	500 aM*	Fluorescence	Graphical barcodes	2	Liu <i>et al.</i> <sup>196</sup>
Microarray (susp.)	HCR	10 pM	Fluorescence	Photonic crystals	3	Bian <i>et al.</i> <sup>198</sup>
Microarray (susp.)	RCA	20 fM	Fluorescence	Photonic crystals	3	Wei <i>et al.</i> <sup>200</sup>
Microarray (susp.)	HCR	1 nM	Fluorescence	Photonic crystals	3	Xu <i>et al.</i> <sup>199</sup>
Microarray (susp.)	DNAzyme	30 pM*	Fluorescence	Particle size	4	Wang <i>et al.</i> <sup>202</sup>
Microarray (susp.)	No	10 fM	SERS	Particle size	3	Shin <i>et al.</i> <sup>203</sup>
Microarray (susp.)	No	2 pM*	Acoustic levitation	Particle size	2	Miyagawa <i>et al.</i> <sup>204</sup>
Microarray (susp.)	No	3 pM	Particle colocalization	Optical + mobility	9	Kim <i>et al.</i> <sup>205</sup>



signatures (red, green and blue, respectively). The second unique feature of this work is kinetic encoding: the particles were also discriminated based on their mobility. For each kind of plasmonic particles, half was functionalized with lipids that could interact with an immobile 2D lipid bilayer, hindering the mobility of the particle. The other half was left free in solution, creating a new dimension of barcoding composed of two levels (mobile and immobile). The third encryption level was linked to the reporting, as target detection was signaled by the colocalization of an immobilized particle with a mobile one. This method allowed for the detection of 9 miRNA targets using only six particle subpopulations. The sensitivity was rather low, however, since the LOD is around 10 pM.

### 3.4 Multiplex microRNA detection from live cells

Although most of the miRNA detection methods presented in this review aim at quantifying miRNAs in cell extracts or bodily fluids, some multiplex methods were also developed to detect miRNAs in live cells. The detection of miRNAs from live cells presents different challenges than detection from biofluids: the quantification method needs to be particularly robust to resist to the complex environment of the cell, while being perfectly biocompatible to avoid damaging it. Most of the reported methods rely on color-coded fluorescent probes quenched by nanoparticles<sup>206,207</sup> or nanosheets.<sup>208–211</sup> Zhou *et al.* designed an assembly of DNA strands forming a tetrahedron that changes its conformation to emit fluorescence upon miRNA hybridization.<sup>212</sup> Similar DNA frameworks were applied by several groups to multiplex miRNA detection thanks to the great versatility and biocompatibility of this approach (Fig. 16).<sup>213,214</sup>

Signal amplification in live cells is particularly challenging, since it requires biocompatibility, which is not required for *ex vivo* detection. Lu *et al.* managed to implement DSNSA in live cells,<sup>215</sup> while Meng and coworkers combined strand-displacement and DNAzyme amplifications in order to increase the sensitivity of their assay.<sup>216</sup> Interestingly, Wang *et al.* took advantage of the cells expression machinery by introducing plasmids promoting the production of fluorescent proteins (*e.g.* GFP, mRFP) once the miRNA is captured.<sup>217</sup> All of the aforementioned techniques rely on fluorescence for detection, and are limited by the one-color-per-target barrier. Wang and coworkers implemented successive cycles composed of an HCR amplification step, fluorescence imaging followed by the degradation of HCR hairpins by DNase I to increase the multiplexing ability of their method to 12.<sup>218</sup> As an alternative to fluorescence, Zhou *et al.* used SERS to detect 2 miRNAs simultaneously in live cells.<sup>219</sup>

## 4 Conclusions and perspectives

Conventional miRNA detection methods suffer from symmetrical limitations: RT-qPCR is highly sensitive, but its multiplex capacity is limited by the lack of spectrally-resolved fluorescent probes, whereas planar microarrays can detect up to thousands of

miRNAs simultaneously but display relatively low sensitivity. In this review, we reported innovative miRNA sensing methods aiming at detecting very low concentrations while being highly multiplexable. Signal overlap still limits the multiplex ability of methods using an independent reporter for each targeted miRNA. This is not only the case for fluorescence-based methods, but also applies to electrochemical or Raman-scattering readouts. Consequently, alternative target indexation methods were implemented to boost the multiplex capacity. Suspension arrays are currently emerging as very promising detection methods. The wide diversity and versatility of functionalizable particles offer high multiplexing potential and compatibility with multiple readout strategies, while the suspension format allows higher sensitivity and throughput than planar microarrays. Although the low concentrations of miRNAs in bodily fluids are still challenging to reach for numerous methods, the field greatly benefited from the design of novel nucleic acid amplification techniques. The development of highly sensitive readout methods, such as SERS, SPR or electrochemical labels, has also been instrumental in the improvement of the sensitivity of assays.

Due to the high sequence homology encountered in the miRNA world, multiplex assays would also need to be highly specific. Different strategies have been explored to increase target specificity. These include the design of selective capture oligonucleotides that discriminate miRNAs taking into account the difference in free energy (using secondary-structured probes or chemical modifications such as LNA). Similarly, specific reporting probes (*e.g.* hydrolysis probes) may be used to discriminate the target sequence from nonspecific reactions. In enzyme-based systems, the choice of the enzyme(s) (polymerase, ligase, restriction enzyme, RNase or other nucleases) is crucial to maximise the assay selectivity with respect to homologous target sequences. Finally, support-assisted designs seem promising leads for improving specificity in multiplexed format.<sup>113,174,220</sup> We refer the readers to a recent review from Ouyang *et al.*, in which the specificity of microRNA detection is thoroughly discussed.<sup>92</sup>

In all the above-mentioned multiplex methods, each miRNA target is individually quantified using independent bio-receptors and data analysis allows to reconstruct the sample profile. These techniques are ideally suited to accurately profile miRNAs and discover novel disease-related signatures. Complementary approaches are focusing on the *in vitro* integration of the data processing step. Conceptually, a DNA circuit is built to integrate the presence or absence of a set of miRNAs, transduce this information *in molecule*, and report an output that depends on the programmable circuits architecture. More than a decade ago, Seelig and coworkers conceived a 11-gate amplification-free DNA circuit that accepts 6 miRNA sequences as input (Let-7c AND miR-124a AND (miR-15a OR miR-10b) AND (miR-143 OR miR-122a)), resulting in the classification of the samples according to the presence or absence of DNA analogues of the targeted sequences.<sup>221</sup> Other groups have cascaded HCR and/or DNAzyme amplification to assemble Boolean logic circuits, using fluorescence,<sup>222</sup> colorimetric<sup>223</sup> or nanopore readout.<sup>224</sup> Although conceptually elegant, these



demonstrations use hundreds of nanomolars to subnanomolar of discrete concentrations of miRNA input, making them unsuitable for clinical applications without substantial sensitivity improvement. Yet another path exploits DNA architectures that emulate neural networks to perform sample classification based on biomolecules concentrations.<sup>221,222</sup> Coupled to PCR and RCA amplification, such approach has recently proven capable of cancer diagnosis from plasma samples:<sup>225</sup> after training an *in silico* classifier from publicly-available miR-seq profile and identified a 4-miRNA signature of non-small cell lung cancer, Zhang *et al.* implemented a DNA classifier that computes the weighted sum of all 4 miRNA targets and returns a yes/no diagnosis. To reach clinically relevant sensitivity, miRNAs from plasma samples were first amplified by RT-PCR and converted to circular single-stranded DNA, subsequently used as input for the molecular computation. Yet to be confirmed, an advantage of these emerging concepts is that the complexity to measure independently miRNA markers is transferred from the technology (microarray, microfluidics, sequencing, *etc.*) to the molecular chemistry, opening the door to miRNA profiling kits for rapid testing, for example for routine screening of cancer diseases from minimally invasive, low-cost procedure, which would expand the arsenal of multiplexed microRNA detection technologies (Table 1).

## Conflicts of interest

G. G., Y. R., T. J., and V. T. are inventors on a patent application related to this work (no. EP 19305670.2, filed 27 May 2019). The authors declare no other conflict of interest.

## Acknowledgements

This research was supported by the Université de Recherche Paris Sciences et Lettres (PSL), the ESPCI-Paris, the Université de Paris, the Centre National de la Recherche Scientifique (CNRS), the Institut National de la Santé et de la Recherche Médicale (INSERM), the Ligue Nationale Contre le Cancer (LNCC, Program “Equipe labelisée LIGUE”; no. EL2016.LNCC/VaT), and the European Research Council (grants 647275 ProFF, 780519 DeepMiR and 949493 MoP-MiP). T. J. received a PhD fellowship from the Conseil Régional d’Ile de France (grant ARDoc 17012687). We thank the SIRIC CARPEM and the Physicancer program (no. PC201423) fundings.

## Notes and references

- 1 R. C. Lee, R. L. Feinbaum and V. Ambros, *Cell*, 1993, **75**, 843–854.
- 2 R. C. Friedman, K. K.-H. Farh, C. B. Burge and D. P. Bartel, *Genome Res.*, 2009, **19**, 92–105.
- 3 A. Fire, S. Xu, M. K. Montgomery, S. A. Kostas, S. E. Driver and C. C. Mello, *Nature*, 1998, **391**, 806–811.
- 4 D. P. Bartel, *Cell*, 2004, **116**, 281–297.
- 5 H. Schwarzenbach, N. Nishida, G. A. Calin and K. Pantel, *Nat. Rev. Clin. Oncol.*, 2014, **11**, 145–156.
- 6 M. Ha and V. N. Kim, *Nat. Rev. Mol. Cell Biol.*, 2014, **15**, 509–524.
- 7 J. Höck and G. Meister, *Genome Biol.*, 2008, **9**, 210.
- 8 J. O’Brien, H. Hayder, Y. Zayed and C. Peng, *Front. Endocrinol.*, 2018, **9**, 402.
- 9 K. Saliminejad, H. R. Khorram Khorshid, S. Soleymani Fard and S. H. Ghaffari, *J. Cell. Physiol.*, 2019, **234**, 5451–5465.
- 10 G. A. Calin, C. D. Dumitru, M. Shimizu, R. Bichi, S. Zupo, E. Noch, H. Aldler, S. Rattan, M. Keating, K. Rai, L. Rassenti, T. Kipps, M. Negrini, F. Bullrich and C. M. Croce, *Proc. Natl. Acad. Sci. U. S. A.*, 2002, **99**, 15524–15529.
- 11 Y. Peng and C. M. Croce, *Signal Transduction Targeted Ther.*, 2016, **1**, 15004.
- 12 A. E. Roser, L. Caldi Gomes, J. Schünemann, F. Maass and P. Lingor, *Front. Neurosci.*, 2018, **12**, 625.
- 13 E. Satake, M. G. Pezzolesi, Z. I. Md Dom, A. M. Smiles, M. A. Niewczas and A. S. Krolewski, *Diabetes*, 2018, **67**, 1013–1023.
- 14 S. Ultimo, G. Zauli, A. M. Martelli, M. Vitale, J. A. McCubrey, S. Capitani and L. M. Neri, *Oncotarget*, 2018, **9**, 17238–17254.
- 15 G. A. Calin and C. M. Croce, *Oncogene*, 2006, **25**, 6202–6210.
- 16 H. Tagawa and M. Seto, *Leukemia*, 2005, **19**, 2013–2016.
- 17 Y. Hayashita, H. Osada, Y. Tatematsu, H. Yamada, K. Yanagisawa, S. Tomida, Y. Yatabe, K. Kawahara, Y. Sekido and T. Takahashi, *Cancer Res.*, 2005, **65**, 9628–9632.
- 18 K. A. O’Donnell, E. A. Wentzel, K. I. Zeller, C. V. Dang and J. T. Mendell, *Nature*, 2005, **435**, 839–843.
- 19 T.-C. Chang, D. Yu, Y.-S. Lee, E. A. Wentzel, D. E. Arking, K. M. West, C. V. Dang, A. Thomas-Tikhonenko and J. T. Mendell, *Nat. Genet.*, 2008, **40**, 43–50.
- 20 L. He, X. He, L. P. Lim, E. de Stanchina, Z. Xuan, Y. Liang, W. Xue, L. Zender, J. Magnus, D. Ridzon, A. L. Jackson, P. S. Linsley, C. Chen, S. W. Lowe, M. A. Cleary and G. J. Hannon, *Nature*, 2007, **447**, 1130–1134.
- 21 Y. Karube, H. Tanaka, H. Osada, S. Tomida, Y. Tatematsu, K. Yanagisawa, Y. Yatabe, J. Takamizawa, S. Miyoshi, T. Mitsudomi and T. Takahashi, *Cancer Sci.*, 2005, **96**, 111–115.
- 22 M. S. Iliou, V. da Silva-Diz, F. J. Carmona, J. Ramalho-Carvalho, H. Heyn, A. Villanueva, P. Muñoz and M. Esteller, *Oncogene*, 2014, **33**, 4003–4015.
- 23 L. He, J. M. Thomson, M. T. Hemann, E. Hernando-Monge, D. Mu, S. Goodson, S. Powers, C. Cordon-Cardo, S. W. Lowe, G. J. Hannon and S. M. Hammond, *Nature*, 2005, **435**, 828–833.
- 24 M. E. Hatley, D. M. Patrick, M. R. Garcia, J. A. Richardson, R. Bassel-Duby, E. van Rooij and E. N. Olson, *Cancer Cell*, 2010, **18**, 282–293.
- 25 J. A. Weber, D. H. Baxter, S. Zhang, D. Y. Huang, K. H. Huang, M. J. Lee, D. J. Galas and K. Wang, *Clin. Chem.*, 2010, **56**, 1733–1741.



26 X. Chen, H. Liang, J. Zhang, K. Zen and C.-Y. Zhang, *Trends Cell Biol.*, 2012, **22**, 125–132.

27 P. S. Mitchell, R. K. Parkin, E. M. Kroh, B. R. Fritz, S. K. Wyman, E. L. Pogosova-Agadjanyan, A. Peterson, J. Noteboom, K. C. O'Briant, A. Allen, D. W. Lin, N. Urban, C. W. Drescher, B. S. Knudsen, D. L. Stirewalt, R. Gentleman, R. L. Vessella, P. S. Nelson, D. B. Martin and M. Tewari, *Proc. Natl. Acad. Sci. U. S. A.*, 2008, **105**, 10513–10518.

28 S. Roush and F. J. Slack, *Trends Cell Biol.*, 2008, **18**, 505–516.

29 H. Dong, J. Lei, L. Ding, Y. Wen, H. Ju and X. Zhang, *Chem. Rev.*, 2013, **113**, 6207–6233.

30 Z. Williams, I. Z. Ben-Dov, R. Elias, A. Mihailovic, M. Brown, Z. Rosenwaks and T. Tuschl, *Proc. Natl. Acad. Sci. U. S. A.*, 2013, **110**, 4255–4260.

31 A. Esquela-Kerscher and F. J. Slack, *Nat. Rev. Cancer*, 2006, **6**, 259–269.

32 S. R. Pfeffer, C. H. Yang and L. M. Pfeffer, *Drug Dev. Res.*, 2015, **76**, 270–277.

33 J. Lu, G. Getz, E. A. Miska, E. Alvarez-Saavedra, J. Lamb, D. Peck, A. Sweet-Cordero, B. L. Ebert, R. H. Mak, A. A. Ferrando, J. R. Downing, T. Jacks, H. R. Horvitz and T. R. Golub, *Nature*, 2005, **435**, 834–838.

34 N. Yanaihara, N. Caplen, E. Bowman, M. Seike, K. Kumamoto, M. Yi, R. M. Stephens, A. Okamoto, J. Yokota, T. Tanaka, G. A. Calin, C.-G. Liu, C. M. Croce and C. C. Harris, *Cancer Cell*, 2006, **9**, 189–198.

35 M. Kahraman, A. Röske, T. Laufer, T. Fehlmann, C. Backes, F. Kern, J. Kohlhaas, H. Schrörs, A. Saiz, C. Zabler, N. Ludwig, P. A. Fasching, R. Strick, M. Rübner, M. W. Beckmann, E. Meese, A. Keller and M. G. Schrauder, *Sci. Rep.*, 2018, **8**, 11584.

36 H. Zhang, M. Zhu, X. Shan, X. Zhou, T. Wang, J. Zhang, J. Tao, W. Cheng, G. Chen, J. Li, P. Liu, Q. Wang and W. Zhu, *Gene*, 2019, **687**, 246–254.

37 T. Ueda, S. Volinia, H. Okumura, M. Shimizu, C. Taccioli, S. Rossi, H. Alder, C.-G. Liu, N. Oue, W. Yasui, K. Yoshida, H. Sasaki, S. Nomura, Y. Seto, M. Kaminishi, G. A. Calin and C. M. Croce, *Lancet Oncol.*, 2010, **11**, 136–146.

38 S. Yerukala Sathipati and S.-Y. Ho, *Sci. Rep.*, 2018, **8**, 16138.

39 X.-H. Shi, X. Li, H. Zhang, R.-Z. He, Y. Zhao, M. Zhou, S.-T. Pan, C.-L. Zhao, Y.-C. Feng, M. Wang, X.-J. Guo and R.-Y. Qin, *Sci. Rep.*, 2018, **8**, 7638.

40 G. Gines, R. Menezes, W. Xiao, Y. Rondelez and V. Taly, *Mol. Aspects Med.*, 2020, **72**, 100832.

41 C. Chen, D. A. Ridzon, A. J. Broomer, Z. Zhou, D. H. Lee, J. T. Nguyen, M. Barbisin, N. L. Xu, V. R. Mahuvakar, M. R. Andersen, K. Q. Lao, K. J. Livak and K. J. Guegler, *Nucleic Acids Res.*, 2005, **33**, e179.

42 R. Shi and V. L. Chiang, *Biotechniques*, 2005, **39**, 519–525.

43 P. Tiberio, M. Callari, V. Angeloni, M. G. Daidone and V. Appierto, *BioMed Res. Int.*, 2015, **2015**, 731479.

44 C. K. Raymond, B. S. Roberts, P. Garrett-Engel, L. P. Lim and J. M. Johnson, *RNA*, 2005, **11**, 1737–1744.

45 P. Mestdagh, N. Hartmann, L. Baeriswyl, D. Andreasen, N. Bernard, C. Chen, D. Cheo, P. D'Andrade, M. DeMayo, L. Dennis, S. Derveaux, Y. Feng, S. Fulmer-Smentek, B. Gerstmayer, J. Gouffon, C. Grimley, E. Lader, K. Y. Lee, S. Luo, P. Mouritzen, A. Narayanan, S. Patel, S. Peiffer, S. Rüberg, G. Schroth, D. Schuster, J. M. Shaffer, E. J. Shelton, S. Silveria, U. Ulmanella, V. Veeramachaneni, F. Staedtler, T. Peters, T. Guettouche, L. Wong and J. Vandesompele, *Nat. Methods*, 2014, **11**, 809–815.

46 V. Benes and M. Castoldi, *Methods*, 2010, **50**, 244–249.

47 C. A. Raabe, T.-H. Tang, J. Brosius and T. S. Rozhdestvensky, *Nucleic Acids Res.*, 2014, **42**, 1414–1426.

48 S. A. Bustin, V. Benes, J. A. Garson, J. Hellemans, J. Huggett, M. Kubista, R. Mueller, T. Nolan, M. W. Pfaffl, G. L. Shipley, J. Vandesompele and C. T. Wittwer, *Clin. Chem.*, 2009, **55**, 611–622.

49 P. Androvic, L. Valihrach, J. Elling, R. Sjoberg and M. Kubista, *Nucleic Acids Res.*, 2017, **45**, e144.

50 J. Zhang, Z. Li, H. Wang, Y. Wang, H. Jia and J. Yan, *Chem. Commun.*, 2011, **47**, 9465–9467.

51 P. Kumar, B. H. Johnston and S. A. Kazakov, *RNA*, 2011, **17**, 365–380.

52 R. T. Fuchs, Z. Sun, F. Zhuang and G. B. Robb, *PLoS One*, 2015, **10**, e0126049.

53 J. Jin, S. Vaud, A. M. Zhelkovsky, J. Posfai and L. A. McReynolds, *Nucleic Acids Res.*, 2016, **44**, e116.

54 E. J. H. Wee and M. Trau, *ACS Sens.*, 2016, **1**, 670–675.

55 S. L. Daubendiek, K. Ryan and E. T. Kool, *J. Am. Chem. Soc.*, 1995, **117**, 7818–7819.

56 D. Liu, S. L. Daubendiek, M. A. Zillman, K. Ryan and E. T. Kool, *J. Am. Chem. Soc.*, 1996, **118**, 1587–1594.

57 S. P. Jonstrup, J. Koch and J. Kjems, *RNA*, 2006, **12**, 1747–1752.

58 H. Takahashi, M. Ohkawachi, K. Horio, T. Kobori, T. Aki, Y. Matsumura, Y. Nakashimada and Y. Okamura, *Sci. Rep.*, 2018, **8**, 7770.

59 T. Krzywkowski and M. Nilsson, *Nucleic Acids Res.*, 2017, **45**, e161.

60 R. Deng, L. Tang, Q. Tian, Y. Wang, L. Lin and J. Li, *Angew. Chem., Int. Ed.*, 2014, **53**, 2389–2393.

61 X. Zhu, Y. Shen, J. Cao, L. Yin, F. Ban, Y. Shu and G. Li, *Chem. Commun.*, 2015, **51**, 10002–10005.

62 T. Fan, Y. Mao, Q. Sun, F. Liu, J. Lin, Y. Liu, J. Cui and Y. Jiang, *Cancer Sci.*, 2018, **109**, 2897–2906.

63 H. Liu, L. Li, L. Duan, X. Wang, Y. Xie, L. Tong, Q. Wang and B. Tang, *Anal. Chem.*, 2013, **85**, 7941–7947.

64 J. Van Ness, L. K. Van Ness and D. J. Galas, *Proc. Natl. Acad. Sci. U. S. A.*, 2003, **100**, 4504–4509.

65 E. Tan, J. Wong, D. Nguyen, Y. Zhang, B. Erwin, L. K. Van Ness, S. M. Baker, D. J. Galas and A. Niemz, *Anal. Chem.*, 2005, **77**, 7984–7992.

66 H. Jia, Z. Li, C. Liu and Y. Cheng, *Angew. Chem., Int. Ed.*, 2010, **49**, 5498–5501.

67 Y. Cheng, L. Dong, J. Zhang, Y. Zhao and Z. Li, *Analyst*, 2018, **143**, 1758–1774.

68 E. Tan, B. Erwin, S. Dames, T. Ferguson, M. Buechel, B. Irvine, K. Voelkerding and A. Niemz, *Biochemistry*, 2008, **47**, 9987–9999.

69 J. Qian, T. M. Ferguson, D. N. Shinde, A. J. Ramírez-Borrero, A. Hintze, C. Adami and A. Niemz, *Nucleic Acids Res.*, 2012, **40**, e87.

70 K. Montagne, G. Gines, T. Fujii and Y. Rondelez, *Nat. Commun.*, 2016, **7**, 13474.

71 G. Gines, R. Menezes, K. Nara, A.-S. Kirstetter, V. Taly and Y. Rondelez, *Sci. Adv.*, 2020, **6**, eaay5952.

72 J. Chen, X. Zhou, Y. Ma, X. Lin, Z. Dai and X. Zou, *Nucleic Acids Res.*, 2016, gkw504.

73 J. Chen, T. An, Y. Ma, B. Situ, D. Chen, Y. Xu, L. Zhang, Z. Dai and X. Zou, *Anal. Chem.*, 2018, **90**, 859–865.

74 D. A. Shagin, D. V. Rebrikov, V. B. Kozhemyako, I. M. Altshuler, A. S. Shcheglov, P. A. Zhulidov, E. A. Bogdanova, D. B. Staroverov, V. A. Rasskazov and S. Lukyanov, *Genome Res.*, 2002, **12**, 1935–1942.

75 V. E. Anisimova, D. V. Rebrikov, D. A. Shagin, V. B. Kozhemyako, N. I. Menzorova, D. B. Staroverov, R. Ziganshin, L. L. Vagner, V. A. Rasskazov, S. A. Lukyanov and A. S. Shcheglov, *BMC Biochem.*, 2008, **9**, 14.

76 B.-C. Yin, Y.-Q. Liu and B.-C. Ye, *J. Am. Chem. Soc.*, 2012, **134**, 5064–5067.

77 Y. Li, J. Zhang, J. Zhao, L. Zhao, Y. Cheng and Z. Li, *Analyst*, 2016, **141**, 1071–1076.

78 H. Zhou, C. Yang, H. Chen, X. Li, Y. Li and X. Fan, *Biosens. Bioelectron.*, 2017, **87**, 552–557.

79 J. Li, S. Yang, C. Zuo, L. Dai, Y. Guo and G. Xie, *ACS Sens.*, 2020, **5**, 970–977.

80 Y. Liu, J. Zhang, J. Tian, X. Fan, H. Geng and Y. Cheng, *Anal. Bioanal. Chem.*, 2017, **409**, 107–114.

81 R. M. Dirks and N. A. Pierce, *Proc. Natl. Acad. Sci. U. S. A.*, 2004, **101**, 15275–15278.

82 S. Venkataraman, R. M. Dirks, P. W. K. Rothemund, E. Winfree and N. A. Pierce, *Nat. Nanotechnol.*, 2007, **2**, 490–494.

83 H. M. T. Choi, J. Y. Chang, L. A. Trinh, J. E. Padilla, S. E. Fraser and N. A. Pierce, *Nat. Biotechnol.*, 2010, **28**, 1208–1212.

84 Q. Guo, F. Bian, Y. Liu, X. Qu, X. Hu and Q. Sun, *Chem. Commun.*, 2017, **53**, 4954–4957.

85 H. M. T. Choi, V. A. Beck and N. A. Pierce, *ACS Nano*, 2014, **8**, 4284–4294.

86 M. Schwarzkopf and N. A. Pierce, *Nucleic Acids Res.*, 2016, gkw503.

87 D. Y. Zhang and E. Winfree, *J. Am. Chem. Soc.*, 2009, **131**, 17303–17314.

88 C. Ma, W. Wang, Z. Li, L. Cao and Q. Wang, *Anal. Biochem.*, 2012, **429**, 99–102.

89 J. Chen, B. Liu, X. Song, P. Tong, H. Yang and L. Zhang, *Sci. China: Chem.*, 2015, **58**, 1906–1911.

90 Y. Liu, T. Shen, J. Li, H. Gong, C. Chen, X. Chen and C. Cai, *ACS Sens.*, 2017, **2**, 1430–1434.

91 A. Válóczi, C. Hornyik, N. Varga, J. Burgýán, S. Kauppinen and Z. Havelda, *Nucleic Acids Res.*, 2004, **32**, e175.

92 T. Ouyang, Z. Liu, Z. Han and Q. Ge, *Anal. Chem.*, 2019, **91**, 3179–3186.

93 E. Arefian, J. Kiani, M. Soleimani, S. A. M. Shariati, S. H. Aghaee-Bakhtiari, A. Atashi, Y. Gheisari, N. Ahmadbeigi, A. M. Banaei-Moghaddam, M. Naderi, N. Namvarasl, L. Good and O. R. Faridani, *Nucleic Acids Res.*, 2011, **39**, e80.

94 A. R. Chandrasekaran, M. MacIsaac, P. Dey, O. Levchenko, L. Zhou, M. Andres, B. K. Dey and K. Halvorsen, *Sci. Adv.*, 2019, **5**, eaau9443.

95 R.-M. Jiang, Y.-S. Chang, S.-J. Chen, J.-H. Chen, H.-C. Chen and P.-L. Chang, *J. Chromatogr. A*, 2011, **1218**, 2604–2610.

96 P. Zhang, Y. Liu, Y. Zhang, C. Liu, Z. Wang and Z. Li, *Chem. Commun.*, 2013, **49**, 10013.

97 K. Wei, J. Zhao, Y. Qin, S. Li, Y. Huang and S. Zhao, *Talanta*, 2018, **189**, 437–441.

98 J. Na, G. W. Shin, H. G. Son, S.-J. V. Lee and G. Y. Jung, *Sci. Rep.*, 2017, **7**, 11396.

99 T. Qi, C. Song, J. He, W. Shen, D. Kong, H. Shi, L. Tan, R. Pan, S. Tang and H. K. Lee, *Anal. Chem.*, 2020, **92**, 5033–5040.

100 S. A. E. Marras, S. Tyagi, D.-O. Antson and F. R. Kramer, *PLoS One*, 2019, **14**, e0213906.

101 A. Rajagopal, A. Scherer, A. Homyk and E. Kartalov, *Anal. Chem.*, 2013, **85**, 7629–7636.

102 F. Moltzahn, A. B. Olshen, L. Baehner, A. Peek, L. Fong, H. Stöppler, J. Simko, J. F. Hilton, P. Carroll and R. Bleloch, *Cancer Res.*, 2011, **71**, 550–560.

103 Z. Jin, D. Geißler, X. Qiu, K. D. Wegner and N. Hildebrandt, *Angew. Chem., Int. Ed.*, 2015, **54**, 10024–10029.

104 X. Qiu and N. Hildebrandt, *ACS Nano*, 2015, **9**, 8449–8457.

105 X. Qiu, J. Guo, Z. Jin, A. Petreto, I. L. Medintz and N. Hildebrandt, *Small*, 2017, **13**, 1700332.

106 J. Guo, C. Mingo, X. Qiu and N. Hildebrandt, *Anal. Chem.*, 2019, **91**, 3101–3109.

107 J. Xu, J. Guo, N. Golob-Schwarzl, J. Haybaeck, X. Qiu and N. Hildebrandt, *ACS Sens.*, 2020, **5**, 1768–1776.

108 X. Qiu, J. Guo, J. Xu and N. Hildebrandt, *J. Phys. Chem. Lett.*, 2018, **9**, 4379–4384.

109 W.-Q. Ye, Y.-X. Wei, Y.-Z. Zhang, C.-G. Yang and Z.-R. Xu, *Anal. Bioanal. Chem.*, 2020, **412**, 647–655.

110 R. Wang, X. Zhao, X. Chen, X. Qiu, G. Qing, H. Zhang, L. Zhang, X. Hu, Z. He, D. Zhong, Y. Wang and Y. Luo, *Anal. Chem.*, 2020, **92**, 2176–2185.

111 Y. Tang, X. He, R. Yuan, X. Liu, Y. Zhao, T. Wang, H. Chen and X. Feng, *Analyst*, 2020, **145**, 4314–4320.

112 L. Cui, X. Lin, N. Lin, Y. Song, Z. Zhu, X. Chen and C. J. Yang, *Chem. Commun.*, 2012, **48**, 194–196.

113 M. Xiao, T. Man, C. Zhu, H. Pei, J. Shi, L. Li, X. Qu, X. Shen and J. Li, *ACS Appl. Mater. Interfaces*, 2018, **10**, 7852–7858.

114 S. Robinson, M. Follo, D. Haenel, M. Maunder, D. Stallmann, L. A. Heger, T. Helbing, D. Duerschmied, K. Peter, C. Bode, I. Ahrens and M. Hortmann, *Acta Pharmacol. Sin.*, 2018, **39**, 1217–1227.

115 S. Robinson, M. Follo, D. Haenel, M. Maunder, D. Stallmann, M. Tewari, D. Duerschmied, K. Peter, C. Bode, I. Ahrens and M. Hortmann, *Int. J. Cardiol.*, 2018, **257**, 247–254.

116 Q. Zhong, S. Bhattacharya, S. Kotsopoulos, J. Olson, V. Taly, A. D. Griffiths, D. R. Link and J. W. Larson, *Lab Chip*, 2011, **11**, 2167.

117 Y. Rondelez and G. Gines, *ACS Sens.*, 2020, **5**, 2430–2437.

118 L. D. Smith, Y. Liu, M. U. Zahid, T. D. Canady, L. Wang, M. Kohli, B. T. Cunningham and A. M. Smith, *ACS Nano*, 2020, **14**, 2324–2335.

119 M. M. Ali, F. Li, Z. Zhang, K. Zhang, D.-K. Kang, J. A. Ankrum, X. C. Le and W. Zhao, *Chem. Soc. Rev.*, 2014, **43**, 3324–3341.

120 Z. Hu, F. Xu, G. Sun, S. Zhang and X. Zhang, *Chem. Commun.*, 2020, **56**, 5409–5412.

121 M. Kühnemund, I. Hernández-Neuta, M. Sharif, M. Cornaglia, M. A. Gijs and M. Nilsson, *Nucleic Acids Res.*, 2017, gkw1324.

122 S. Barberán-Soler, J. M. Vo, R. E. Hogans, A. Dallas, B. H. Johnston and S. A. Kazakov, *Genome Biol.*, 2018, **19**, 105.

123 M. R. Friedländer, W. Chen, C. Adamidi, J. Maaskola, R. Einspanier, S. Knespel and N. Rajewsky, *Nat. Biotechnol.*, 2008, **26**, 407–415.

124 V. P. Dave, T. A. Ngo, A.-K. Pernestig, D. Tilevik, K. Kant, T. Nguyen, A. Wolff and D. D. Bang, *Lab. Invest.*, 2019, **99**, 452–469.

125 T. C. Glenn, *Mol. Ecol. Resour.*, 2011, **11**, 759–769.

126 S. Alon, F. Vigneault, S. Eminaga, D. C. Christodoulou, J. G. Seidman, G. M. Church and E. Eisenberg, *Genome Res.*, 2011, **21**, 1506–1511.

127 Y.-J. Chen, C. N. Takahashi, L. Organick, C. Bee, S. D. Ang, P. Weiss, B. Peck, G. Seelig, L. Ceze and K. Strauss, *Nat. Commun.*, 2020, **11**, 3264.

128 S. Tam, R. de Borja, M.-S. Tsao and J. D. McPherson, *Lab. Invest.*, 2014, **94**, 350–358.

129 Q. Yang, J. Lin, M. Liu, R. Li, B. Tian, X. Zhang, B. Xu, M. Liu, X. Zhang, Y. Li, H. Shi and L. Wu, *Sci. Adv.*, 2016, **2**, e1501482.

130 A. M. L. Coenen-Stass, H. Sork, S. Gatto, C. Godfrey, A. Bhomra, K. Krjutškov, J. R. Hart, J. O. Westholm, L. O'Donovan, A. Roos, H. Lochmüller, P. L. Puri, S. El Andaloussi, M. J. A. Wood and T. C. Roberts, *Mol. Ther.–Nucleic Acids*, 2018, **13**, 1–15.

131 C. Yang, B. Dou, K. Shi, Y. Chai, Y. Xiang and R. Yuan, *Anal. Chem.*, 2014, **86**, 11913–11918.

132 Y. Chang, Z. Wu, Q. Sun, Y. Zhuo, Y. Chai and R. Yuan, *Anal. Chem.*, 2019, **91**, 8123–8128.

133 S. Xu, Y. Chang, Z. Wu, Y. Li, R. Yuan and Y. Chai, *Biosens. Bioelectron.*, 2020, **149**, 111848.

134 W. Zhu, X. Su, X. Gao, Z. Dai and X. Zou, *Biosens. Bioelectron.*, 2014, **53**, 414–419.

135 J. Wang, Z. Lu, H. Tang, L. Wu, Z. Wang, M. Wu, X. Yi and J. Wang, *Anal. Chem.*, 2017, **89**, 10834–10840.

136 S. Azzouzi, Z. Fredj, A. P. F. Turner, M. B. Ali and W. C. Mak, *ACS Sens.*, 2019, **4**, 326–334.

137 R. Liu, S. Zhang, C. Wei, Z. Xing, S. Zhang and X. Zhang, *Acc. Chem. Res.*, 2016, **49**, 775–783.

138 S. Zhang, R. Liu, Z. Xing, S. Zhang and X. Zhang, *Chem. Commun.*, 2016, **52**, 14310–14313.

139 E. C. Le, Ru, E. Blackie, M. Meyer and P. G. Etchegoin, *J. Phys. Chem. C*, 2007, **111**, 13794–13803.

140 J. Su, D. Wang, L. Nörbel, J. Shen, Z. Zhao, Y. Dou, T. Peng, J. Shi, S. Mathur, C. Fan and S. Song, *Anal. Chem.*, 2017, **89**, 2531–2538.

141 W. Zhou, Y.-F. Tian, B.-C. Yin and B.-C. Ye, *Anal. Chem.*, 2017, **89**, 6120–6128.

142 H.-N. Wang, B. M. Crawford, A. M. Fales, M. L. Bowie, V. L. Seewaldt and T. Vo-Dinh, *J. Phys. Chem. C*, 2016, **120**, 21047–21055.

143 W. H. Kim, J. U. Lee, S. Song, S. Kim, Y. J. Choi and S. J. Sim, *Analyst*, 2019, **144**, 1768–1776.

144 G. K. Geiss, R. E. Bumgarner, B. Birditt, T. Dahl, N. Dowidar, D. L. Dunaway, H. P. Fell, S. Ferree, R. D. George, T. Grogan, J. J. James, M. Maysuria, J. D. Mitton, P. Oliveri, J. L. Osborn, T. Peng, A. L. Ratcliffe, P. J. Webster, E. H. Davidson, L. Hood and K. Dimitrov, *Nat. Biotechnol.*, 2008, **26**, 317–325.

145 I. Amit, M. Garber, N. Chevrier, A. P. Leite, Y. Donner, T. Eisenhaure, M. Guttman, J. K. Grenier, W. Li, O. Zuk, L. A. Schubert, B. Birditt, T. Shay, A. Goren, X. Zhang, Z. Smith, R. Deering, R. C. McDonald, M. Cabilio, B. E. Bernstein, J. L. Rinn, A. Meissner, D. E. Root, N. Hacohen and A. Regev, *Science*, 2009, **326**, 257–263.

146 Y.-H. Su, E. Li, G. K. Geiss, W. J. R. Longabaugh, A. Krämer and E. H. Davidson, *Dev. Biol.*, 2009, **329**, 410–421.

147 W. Wang, M. Corrigan-Cummins, J. Hudson, I. Maric, O. Simakova, S. S. Neelapu, L. W. Kwak, J. E. Janik, B. Gause, E. S. Jaffe and K. R. Calvo, *Haematologica*, 2012, **97**, 586–594.

148 C. Foye, I. K. Yan, W. David, N. Shukla, Y. Habboush, L. Chase, K. Ryland, V. Kesari and T. Patel, *PLoS One*, 2017, **12**, e0189165.

149 A. Kozomara, M. Birgaoanu and S. Griffiths-Jones, *Nucleic Acids Res.*, 2019, **47**, D155–D162.

150 A. Giannoudis, K. Clarke, R. Zakaria, D. Varešlija, M. Farahani, L. Rainbow, A. Platt-Higgins, S. Ruthven, K. A. Brougham, P. S. Rudland, M. D. Jenkinson, L. S. Young, F. Falciani and C. Palmieri, *Sci. Rep.*, 2019, **9**, 18518.

151 S. B. Dejene, A. W. Ohman, W. Du, D. Randhawa, A. Bradley, N. Yadav, K. M. Elias, D. M. Dinulescu and S. R. Setlur, *Cancer Med.*, 2019, **8**, 6709–6716.

152 E. A. Hunt, D. Broyles, T. Head and S. K. Deo, *Annu. Rev. Anal. Chem.*, 2015, **8**, 217–237.

153 M. Guleđ, L. Lahti, P. M. Lindholm, K. Salmenkivi, I. Bagwan, A. G. Nicholson and S. Knuutila, *Genes, Chromosomes Cancer*, 2009, **48**, 615–623.

154 J.-J. Zhao, J. Yang, J. Lin, N. Yao, Y. Zhu, J. Zheng, J. Xu, J. Q. Cheng, J.-Y. Lin and X. Ma, *Childs Nerv. Syst.*, 2009, **25**, 13–20.

155 E. M. Southern, *Methods Mol. Biol.*, 2001, **170**, 1–15.

156 T. Babak, *RNA*, 2004, **10**, 1813–1819.

157 J. M. Thomson, J. Parker, C. M. Perou and S. M. Hammond, *Nat. Methods*, 2004, **1**, 47–53.

158 R.-Q. Liang, *Nucleic Acids Res.*, 2005, **33**, e17.

159 C.-G. Liu, G. A. Calin, B. Meloon, N. Gamliel, C. Sevignani, M. Ferracin, C. D. Dumitru, M. Shimizu, S. Zupo, M. Dono,



H. Alder, F. Bullrich, M. Negrini and C. M. Croce, *Proc. Natl. Acad. Sci. U. S. A.*, 2004, **101**, 9740–9744.

160 S. Baskerville and D. P. Bartel, *RNA*, 2005, **11**, 241–247.

161 E. A. Miska, E. Alvarez-Saavedra, M. Townsend, A. Yoshii, N. Sestan, P. Rakic, M. Constantine-Paton and H. R. Horvitz, *Genome Biol.*, 2004, **5**, R68.

162 J. Q. Yin, R. C. Zhao and K. V. Morris, *Trends Biotechnol.*, 2008, **26**, 70–76.

163 M. Castoldi, *RNA*, 2006, **12**, 913–920.

164 S. Roy, J. H. Soh and J. Y. Ying, *Biosens. Bioelectron.*, 2016, **75**, 238–246.

165 J. U. Lee, W. H. Kim, H. S. Lee, K. H. Park and S. J. Sim, *Small*, 2019, **15**, 1804968.

166 X. Liu, R. Tian, J. Gao, D. Liu and Z. Wang, *Analyst*, 2017, **142**, 4529–4535.

167 A. Sguassero, A. Artiga, C. Morasso, R. R. Jimenez, R. M. Rapún, R. Mancuso, S. Agostini, A. Hernis, A. Abols, A. Liné, A. Gualerzi, S. Picciolini, M. Bedoni, M. Rovaris, F. Gramatica, J. M. de la Fuente and R. Vanna, *Anal. Bioanal. Chem.*, 2019, **411**, 1873–1885.

168 W. K. Yeung, H.-Y. Chen, J.-J. Sun, T.-H. Hsieh, M. Z. Mousavi, H.-H. Chen, K.-L. Lee, H. Lin, P.-K. Wei and J.-Y. Cheng, *Analyst*, 2018, **143**, 4715–4722.

169 A. J. Qavi, J. T. Kindt, M. A. Gleeson and R. C. Bailey, *Anal. Chem.*, 2011, **83**, 5949–5956.

170 S. Hofmann, Y. Huang, P. Paulicka, A. Kappel, H. A. Katus, A. Keller, B. Meder, C. F. Stähler and W. Gumbrecht, *Anal. Chem.*, 2015, **87**, 12104–12111.

171 Y. Wen, L. Li, J. Li, M. Lin, G. Liu, W. Liang, L. Xu, Y. Li, X. Zuo, S. Ren and Y. Zhu, *Anal. Chem.*, 2020, **92**, 4498–4503.

172 H. Lee, J. Lee, S.-G. Lee and P. S. Doyle, *Anal. Chem.*, 2020, **92**, 5750–5755.

173 W. Choi, S. Y. Yeom, J. Kim, S. Jung, S. Jung, T. S. Shim, S. K. Kim, J. Y. Kang, S. H. Lee, I.-J. Cho, J. Choi and N. Choi, *Biosens. Bioelectron.*, 2018, **101**, 235–244.

174 S. Jung, W. J. Kim, B. K. Kim, J. Kim, M. J. Kim, K. P. Kim and S. K. Kim, *Biosens. Bioelectron.*, 2020, **163**, 112301.

175 K. Hashimoto, M. Inada and K. Ito, *Anal. Chem.*, 2019, **91**, 3227–3232.

176 K. Hosokawa, T. Sato, Y. Sato and M. Maeda, *Anal. Sci.*, 2010, **26**, 1053–1057.

177 A. Mader, U. Riehle, T. Brandstetter, E. Stickeler and J. Ruehe, *Anal. Chim. Acta*, 2012, **754**, 1–7.

178 J. P. Nolan and L. A. Sklar, *Trends Biotechnol.*, 2002, **20**, 9–12.

179 L. Cohen, M. R. Hartman, A. Amardey-Wellington and D. R. Walt, *Nucleic Acids Res.*, 2017, **45**, e137.

180 F. Causa, A. Aliberti, A. M. Cusano, E. Battista and P. A. Netti, *J. Am. Chem. Soc.*, 2015, **137**, 1758–1761.

181 X. Qu, H. Jin, Y. Liu and Q. Sun, *Anal. Chem.*, 2018, **90**, 3482–3489.

182 J.-J. Wang, C. Zheng, Y.-Z. Jiang, Z. Zheng, M. Lin, Y. Lin, Z.-L. Zhang, H. Wang and D.-W. Pang, *Anal. Chem.*, 2020, **92**, 830–837.

183 D. Li, Y. Wang, C. Lau and J. Lu, *Anal. Chem.*, 2014, **86**, 10148–10156.

184 G. Tao, T. Lai, X. Xu, Y. Ma, X. Wu, X. Pei, F. Liu and N. Li, *Anal. Chem.*, 2020, **92**, 3697–3706.

185 D. M. Rissin, C. W. Kan, T. G. Campbell, S. C. Howes, D. R. Fournier, L. Song, T. Piech, P. P. Patel, L. Chang, A. J. Rivnak, E. P. Ferrell, J. D. Randall, G. K. Provuncher, D. R. Walt and D. C. Duffy, *Nat. Biotechnol.*, 2010, **28**, 595–599.

186 D. M. Rissin, D. R. Fournier, T. Piech, C. W. Kan, T. G. Campbell, L. Song, L. Chang, A. J. Rivnak, P. P. Patel, G. K. Provuncher, E. P. Ferrell, S. C. Howes, B. A. Pink, K. A. Minnehan, D. H. Wilson and D. C. Duffy, *Anal. Chem.*, 2011, **83**, 2279–2285.

187 L. Song, D. W. Hanlon, L. Chang, G. K. Provuncher, C. W. Kan, T. G. Campbell, D. R. Fournier, E. P. Ferrell, A. J. Rivnak, B. A. Pink, K. A. Minnehan, P. P. Patel, D. H. Wilson, M. A. Till, W. A. Faubion and D. C. Duffy, *J. Immunol. Methods*, 2011, **372**, 177–186.

188 D. Wu, M. D. Milutinovic and D. R. Walt, *Analyst*, 2015, **140**, 6277–6282.

189 L. Song, D. Shan, M. Zhao, B. A. Pink, K. A. Minnehan, L. York, M. Gardel, S. Sullivan, A. F. Phillips, R. B. Hayman, D. R. Walt and D. C. Duffy, *Anal. Chem.*, 2013, **85**, 1932–1939.

190 S. Jung, J. Kim, D. J. Lee, E. H. Oh, H. Lim, K. P. Kim, N. Choi, T. S. Kim and S. K. Kim, *Sci. Rep.*, 2016, **6**, 22975.

191 S. C. Chapin and P. S. Doyle, *Anal. Chem.*, 2011, **83**, 7179–7185.

192 H. Lee, S. J. Shapiro, S. C. Chapin and P. S. Doyle, *Anal. Chem.*, 2016, **88**, 3075–3081.

193 M. B. Nagarajan, A. M. Tentori, W. C. Zhang, F. J. Slack and P. S. Doyle, *Anal. Chem.*, 2018, **90**, 10279–10285.

194 N. Juthani and P. S. Doyle, *Analyst*, 2020, **145**, 5134–5140.

195 J. J. Kim, L. Chen and P. S. Doyle, *Lab Chip*, 2017, **17**, 3120–3128.

196 S. Liu, H. Fang, C. Sun, N. Wang and J. Li, *Analyst*, 2018, **143**, 5137–5144.

197 Y. Xia, B. Gates, Y. Yin and Y. Lu, *Adv. Mater.*, 2000, **12**, 693–713.

198 F. Bian, J. Wu, H. Wang, L. Sun, C. Shao, Y. Wang, Z. Li, X. Wang and Y. Zhao, *Small*, 2018, **14**, 1803551.

199 Y. Xu, H. Wang, C. Luan, F. Fu, B. Chen, H. Liu and Y. Zhao, *Adv. Funct. Mater.*, 2018, **28**, 1704458.

200 X. Wei, F. Bian, X. Cai, Y. Wang, L. Cai, J. Yang, Y. Zhu and Y. Zhao, *Anal. Chem.*, 2020, **92**, 6121–6127.

201 R. Bilan, A. Ametzazurra, K. Brazhnik, S. Escorza, D. Fernández, M. Uriábarri, I. Nabiev and A. Sukhanova, *Sci. Rep.*, 2017, **7**, 44668.

202 N. Wang, L. Song, T. Deng and J. Li, *Anal. Chim. Acta*, 2020, **1140**, 69–77.

203 K. Shin, J. Choi, Y. Kim, Y. Lee, J. Kim, S. Lee and H. Chung, *J. Chromatogr. A*, 2018, **1556**, 97–102.

204 A. Miyagawa, M. Harada and T. Okada, *Anal. Chem.*, 2018, **90**, 13729–13735.

205 S. Kim, J.-E. Park, W. Hwang, J. Seo, Y.-K. Lee, J.-H. Hwang and J.-M. Nam, *J. Am. Chem. Soc.*, 2017, **139**, 3558–3566.

206 H. Lu, K. Guo, Y. Cao, F. Yang, D. Wang, L. Dou, Y. Liu and H. Dong, *Anal. Chem.*, 2020, **92**, 1850–1855.



207 J. Li, J. Huang, X. Yang, Y. Yang, K. Quan, N. Xie, Y. Wu, C. Ma and K. Wang, *Nanotheranostics*, 2018, **2**, 96–105.

208 Q. Lu, D. Ericson, Y. Song, C. Zhu, R. Ye, S. Liu, J. A. Spernyak, D. Du, H. Li, Y. Wu and Y. Lin, *ACS Appl. Mater. Interfaces*, 2017, **9**, 23325–23332.

209 Y. Wu, J. Han, P. Xue, R. Xu and Y. Kang, *Nanoscale*, 2015, **7**, 1753–1759.

210 J. Yu, S. He, C. Shao, H. Zhao, J. Li and L. Tian, *Nanoscale*, 2018, **10**, 7067–7076.

211 X. Liao, Q. Wang and H. Ju, *Chem. Commun.*, 2014, **50**, 13604–13607.

212 W. Zhou, D. Li, C. Xiong, R. Yuan and Y. Xiang, *ACS Appl. Mater. Interfaces*, 2016, **8**, 13303–13308.

213 Z. Zhou, Y. S. Sohn, R. Nechushtai and I. Willner, *ACS Nano*, 2020, **14**, 9021–9031.

214 F. Yang, Y. Cheng, Y. Zhang, W. Wei, H. Dong, H. Lu and X. Zhang, *Anal. Chem.*, 2020, **92**, 4411–4418.

215 H. Lu, K. Guo, Y. Cao, F. Yang, D. Wang, L. Dou, Y. Liu and H. Dong, *Anal. Chem.*, 2020, **92**, 1850–1855.

216 X. Meng, K. Zhang, W. Dai, Y. Cao, F. Yang, H. Dong and X. Zhang, *Chem. Sci.*, 2018, **9**, 7419–7425.

217 S. Wang, N. J. Emery and A. P. Liu, *ACS Synth. Biol.*, 2019, **8**, 1079–1088.

218 Z. Wang, L. Qi, Y. Yang, M. Lu, K. Xie, X. Zhao, E. H. C. Cheung, Y. Wang, X. Jiang, W. Zhang, L. Huang, X. Wang and P. Shi, *Sci. Adv.*, 2020, **6**, eaba4971.

219 W. Zhou, Q. Li, H. Liu, J. Yang and D. Liu, *ACS Nano*, 2017, **11**, 3532–3541.

220 S. Jung, B. K. Kim, S. Lee, S. Yoon, H.-I. Im and S. K. Kim, *Sens. Actuators, B*, 2018, **262**, 118–124.

221 G. Seelig, D. Soloveichik, D. Y. Zhang and E. Winfree, *Science*, 2006, **314**, 1585–1588.

222 K. Quan, J. Li, J. Wang, N. Xie, Q. Wei, J. Tang, X. Yang, K. Wang and J. Huang, *Chem. Sci.*, 2019, **10**, 1442–1449.

223 X. Ma, X. Chen, Y. Tang, R. Yan and P. Miao, *ACS Appl. Mater. Interfaces*, 2019, **11**, 41157–41164.

224 S. Zhang, J. Cheng, W. Shi, K.-B. Li, D.-M. Han and J.-J. Xu, *Anal. Chem.*, 2020, **92**, 5952–5959.

225 C. Zhang, Y. Zhao, X. Xu, R. Xu, H. Li, X. Teng, Y. Du, Y. Miao, H. C. Lin and D. Han, *Nat. Nanotechnol.*, 2020, **15**, 709–715.

226 R. Ishihara, K. Hasegawa, K. Hosokawa and M. Maeda, *Anal. Sci.*, 2015, **31**, 573–576.

227 C. Wang, Q. Ding, P. Plant, M. Basheer, C. Yang, E. Tawedrous, A. Krizova, C. Boulos, M. Farag, Y. Cheng and G. M. Yousef, *Clin. Biochem.*, 2019, **67**, 54–59.

